Conversion of σ,η-Allenyl Group into a σ,σ-(Diphenylphosphino)allyl and a Hexa-1,3,5-triene-2,6-diyl Ligand at a Diiron Center†

Simon Doherty,*,‡ Graeme Hogarth,§ Mark Waugh,‡ William Clegg,‡ and Mark R. J. Elsegood‡

Departments of Chemistry, Bedson Building, The University of Newcastle upon Tyne, Newcastle upon Tyne NE1 7RU, U.K., and University College London, 20 Gordon Street, London WC1H 0AJ, U.K.

Received August 14, 2000

Thermolysis of a toluene solution of $[Fe_2(CO)_5(PPh_3)(\mu\text{-}PPh_2)\{\mu\text{-}\eta^1{:}\eta^2{}_{\alpha,\beta}\text{-}(H)C_\alpha{=}C_\beta{=}C_\gamma R_2\}]$ (R = H, **4a**; R = Me, **4b**), obtained via CO substitution in $[Fe_2(CO)_6(\mu\text{-}PPh_2)\{\mu\text{-}\eta^1{:}\eta^2{}_{\alpha,\beta}\text{-}(H)C_\alpha{=}C_\beta{=}C_\gamma R_2\}]$ (R = H, **1a**; R = Me, **1b**), results in regiospecific 1,2-migration of the phosphido bridge to the α-carbon of the σ,η-allenyl group to give $[Fe_2(CO)_5(PPh_3)\{\mu\text{-}\eta^1{:}\eta^3\text{-}(Ph_2P)HCCCR_2\}]$ (R = H, **5a**; R = Me, **5b**) and, in the case of R = H, $[Fe_2(CO)_4(PPh_3)_2\{\mu\text{-}\eta^1{:}\eta^3\text{-}(PPh_2)HCCCH_2\}]$ (R = H, **6**). Single-crystal X-ray analysis of **6** revealed that the $Ph_2PC(H)C{=}CH_2$ fragment can be considered as a 1-diphenylphosphino-substituted propene-1,2-diyl group which functions as a six-electron donor. Thermolysis of a toluene solution of $[Fe_2(CO)_6(\mu\text{-}PPh_2)\{\mu\text{-}\eta^1{:}\eta^2{}_{\alpha,\beta}\text{-}(H)C_\alpha{=}C_\beta{=}C_\gamma Me_2\}]$ (**1b**) results in a similar transformation to give $[Fe_2(CO)_6\{\mu\text{-}\eta^1{:}\eta^3\text{-}(Ph_2P)HCCCMe_2\}]$ (**7**). In contrast, in the absence of PPh_3, thermolysis of a toluene solution of $[Fe_2(CO)_6(\mu\text{-}PPh_2)\{\mu\text{-}\eta^1{:}\eta^2{}_{\alpha,\beta}\text{-}(H)C_\alpha{=}C_\beta{=}C_\gamma H_2\}]$ (**1a**) results in intermolecular carbon−carbon coupling of two $\mu\text{-}\eta^1{:}\eta^2$-allenyl groups to give $[Fe_4(CO)_{11}(\mu\text{-}PPh_2)_2\{\mu\text{-}\eta^1{:}\eta^2{:}\eta^1{:}\eta^2{:}\eta^2\text{-}(H)C{=}CHCHCHC{=}CH_2\}]$ (**8**). Deuterium labeling studies have been used to identify the most likely regioselectivity of carbon−carbon coupling and hydrogen migration. A single-crystal X-ray study of **8** revealed a polyunsaturated hexa-1,3,5-trien-2,6-diyl chain, coordinated to one bimetallic unit as a $\mu\text{-}\eta^1{:}\eta^2$-alkenyl group and to the other as a $\mu\text{-}\eta^1{:}\eta^2{:}\eta^2$-butadien-2-yl group. Solution NMR studies reveal that both **4a** and **4b** exist as rapidly interconverting mixtures of two isomers (**4a$_1$** + **4a$_2$** and **4b$_1$** + **4b$_2$**). The free energy of activation associated with this exchange ($\Delta G^\ddagger = 15.9 \pm 0.2$ kcal mol^{-1}, **4a**; $\Delta G^\ddagger = 16.1 \pm 0.2$ kcal mol^{-1}, **4b**) is consistent with a flipping motion of the allenyl ligand that interchanges the isomer with the triphenylphosphine attached to the σ-bonded iron with that in which the phosphine is attached to the η^2-bonded iron. A value of 1.2 kcal mol^{-1} has been estimated for the difference in free energy between isomers **4a$_1$** and **4a$_2$**. Full structural details of the compounds **4a$_1$**, **4b$_2$**, and **6**−**8** are reported.

Introduction

Carbon−carbon coupling reactions of σ,η unsaturated hydrocarbyl ligands are emerging as a useful strategy for the synthesis of new multisite-bound polycarbons,[1] which may be used to construct two- and three-dimensional multimetallic arrays or reacted further to generate more elaborate organic architectures. One approach that has proven particularly effective for the generation of new polycarbon structures is the addition of a carbene to a coordinated carbon−carbon multiple bond.[2] An alternative approach to the synthesis of polycarbon derivatives involves the regiospecific head-to-head intermolecular coupling of $\mu\text{-}\eta^1{:}\eta^2$-alkynyl complexes of the type $[M_2(CO)_6(\mu\text{-}PPh_2)(\mu\text{-}C{\equiv}CR)]$ (M = Fe, Ru; R = Ph, Bu^t, C≡CPh). For example, Carty and Mays independently reported that the thermolysis of $[Fe_2(CO)_6(\mu\text{-}PPh_2)(\mu\text{-}\eta^1{:}\eta^2\text{-}C{\equiv}CPh)]$ results in regioselective dimerization via head-to-head carbon−carbon coupling to give $[Fe_4(CO)_8(\mu\text{-}PPh_2)_2(\mu_4\text{-}\eta^1{:}\eta^1{:}\eta^1{:}\eta^1{:}\eta^2{:}\eta^2{:}\eta^2{:}\eta^2\text{-}PhCCCCPh)]$, in which the two face-capping alkynyl groups are coupled through the center of the Fe_4 plane.[3] Likewise, thermolysis of $[Ru_2(CO)_6(\mu\text{-}PPh_2)(\mu\text{-}\eta^1{:}\eta^2\text{-}C{\equiv}$

* To whom correspondence should be addressed. E-mail: simon.doherty@newcastle.ac.uk.

† Dedicated to Arthur J. Carty on the occasion of his 60th birthday, with great admiration and sincere thanks.

‡ The University of Newcastle upon Tyne.

§ University College London.

(1) (a) Chi, Y.; Wu, H. L.; Peng, S.-M.; Lee, G.-H. *J. Chem. Soc., Dalton Trans.* **1997**, 1931. (b) Shiu, C. W.; Chi, L.; Chung, C.; Peng, S.-M.; Lee, G.-H. *Organometallics* **1998**, *17*, 2970. (c) Hwang, D.-K.; Lin, P.-J.; Chi, Y.; Peng, S.-M.; Lee, G.-H. *J. Chem. Soc., Dalton Trans.* **1991**, 2161. (d) Akita, M.; Sugimoto, S.; Terada, M.; Moro-oka, Y. *J. Organomet. Chem.* **1993**, *447*, 103. (e) Akita, M.; Kato, S.; Terada, M.; Masaki, Y.; Tanaka, M.; Moro-oka, Y. *Organometallics* **1997**, *16*, 2392. (f) Matsuzaka, H.; Hirayama, Y.; Nishio, M.; Mizove, Y.; Hidai, M. *Organometallics* **1993**, *12*, 36. (g) Kaneko, Y.; Suzuki, A.; Nishiyama, T.; Suzuki, T.; Isobe, K. *Organometallics* **1998**, *17*, 4875. (h) Kaneko, Y.; Suzuki, A.; Isobe, K.; Maitlis, P. *J. Organomet. Chem.* **1998**, *554*, 155. (i) Blenkiron, P.; Enright, G. D.; Low, P. J.; Corrigan, J. F.; Taylor, N. J.; Chi, Y.; Saillard, J.-Y.; Carty, A. J. *Organometallics* **1998**, *17*, 2447.

(2) (a) Blenkiron, P.; Enright, G. D.; Taylor, N. J. Carty, A. J. *Organometallics* **1996**, *15*, 2855. (b) Nucciarone, D.; Taylor, N. J.; Carty, A. J. *Organometallics* **1986**, *5*, 1179. (c) Nucciarone, D.; MacLaughlin, S. A.; Taylor, N. J.; Carty, A. J. *Organometallics* **1988**, *7*, 106. (d) Day, M.; Freeman, W.; Hardcastle, K. I.; Isomaki, M.; Kabir, S. E.; McPhillips, T.; Rosenberg, E.; Scott, L. G. Wolf, E. *Organometallics* **1992**, *11*, 3376.

10.1021/om000702x CCC: $19.00
Publication on Web 11/17/2000

Scheme 1

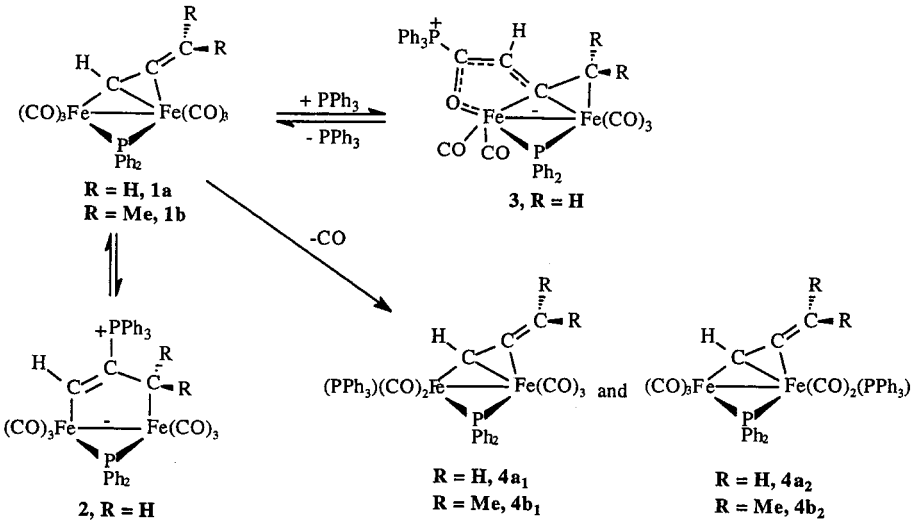

CR)] (R = Ph, Bu^t) also results in dimerization via ynyl coupling, although the nature of the product depends markedly on the alkynyl substituent.[4] It should be noted, however, that the thermolysis of σ,η-alkynyl complexes does not always result in dimerization. For example, thermolysis of $[Fe_2(CO)_6(\mu\text{-}PPh_2)(\mu\text{-}C{\equiv}CBu^t)]$ gave the alkenyl complex $[Fe_2(CO)_4(\mu\text{-}PPh_2)(\mu\text{-}o\text{-}Ph_2PC_6H_4C{=}CHBu^t)]$ and the unusual enyne-bridged $[Fe_3(CO)_4(\mu_3\text{-}o\text{-}PhPC_6H_4PPh)\{\mu_3\text{-}C(Bu^t)CCH{=}CBu^t\text{-}\eta^6\text{-}C_6H_5\}]$, both of which require a complex sequence of transformations including C−C bond formation and C−H and C−P bond cleavage and re-formation.[5]

In an attempt to extend these intermolecular coupling reactions to other σ,σ-bound unsaturated hydrocarbons, we have studied the thermolysis of the allenyl complexes $[Fe_2(CO)_6(\mu\text{-}PPh_2)\{\mu\text{-}C(H){=}C{=}CR_2\}]$ (R = H, Me) and $[Fe_2(CO)_5(PPh_3)(\mu\text{-}PPh_2)\{\mu\text{-}C(H){=}C{=}CR_2\}]$. Surprisingly, we found only one example of allenyl dimerization; all the remaining transformations involved intramolecular P−C bond formation to give 1-diphenylphosphino-substituted $\sigma\text{-}\eta^3$-allyl-bridged complexes. Herein we report two new transformations of binuclear σ,η-allenyl complexes: (i) the regiospecific 1,2-migration of the phosphido bridge to the α-carbon of a bridging allenyl group and (ii) the regiospecific intermolecular coupling of two $\mu\text{-}\eta^1{:}\eta^2$-allenyl groups to give a hexa-1,3,5-triene-2,6-diyl-linked tetrairon complex.

Results and Discussion

Synthesis, Structure, and Fluxionality of $[Fe_2(CO)_5(PPh_3)(\mu\text{-}PPh_2)\{\mu\text{-}\eta^1{:}\eta^2\text{-}(H)C_\alpha{=}C_\beta{=}C_\gamma R_2\}]$ (R = H, 1a; R = Me, 1b). Recently, we reported that the σ,η-allenyl complex $[Fe_2(CO)_6(\mu\text{-}PPh_2)\{\mu\text{-}\eta^1{:}\eta^2{}_{\alpha,\beta}\text{-}(H)C_\alpha{=}C_\beta{=}C_\gamma H_2\}]$ (**1a**) reacts with PPh_3 to give the dimetallacyclopentene $[Fe_2(CO)_6(\mu\text{-}PPh_2)\{\mu\text{-}\eta^1{:}\eta^1\text{-}HC{=}C(PPh_3)\text{-}CH_2\}]$ (**2**), and this readily isomerizes to the zwitterionic α-phosphonium alkoxide $[Fe_2(CO)_5(\mu\text{-}PPh_2)\{\mu\text{-}\eta^1{:}\eta^2\text{-}PPh_3C(O)CHC{=}CH_2\}]$ (**3**) via an unusual carbonyl−phosphine−allenyl coupling sequence, a transformation that involves a complex dissociative equilibrium between **1** and PPh_3.[6] We have now found that toluene solutions of **3** smoothly decarbonylate over several days to afford $[Fe_2(CO)_5(PPh_3)(\mu\text{-}PPh_2)\{\mu\text{-}\eta^1{:}\eta^2\text{-}(H)C{=}C{=}CH_2\}]$ (**4a**), a transformation that occurs more rapidly (approximately 1 h) at reflux. Not surprisingly, **4a** can also be prepared by heating toluene solutions of **1** and PPh_3 for extended periods. Similarly, $[Fe_2(CO)_6(\mu\text{-}PPh_2)\{\mu\text{-}\eta^1{:}\eta^2{}_{\alpha,\beta}\text{-}(H)C_\alpha{=}C_\beta{=}C_\gamma Me_2\}]$ (**1b**), prepared from $[Fe_2(CO)_6(\mu\text{-}CO)(\mu\text{-}PPh_2)]Na$ and 1-chloro-1-methyl-3-butyne in a manner analogous to that for **1a**, reacts with PPh_3 in toluene to give $[Fe_2(CO)_5(PPh_3)(\mu\text{-}PPh_2)\{\mu\text{-}\eta^1{:}\eta^2\text{-}(H)C{=}C{=}CMe_2\}]$ (**4b**).

The $^{31}P\{^1H\}$, ^1H, and $^{13}C\{^1H\}$ NMR spectra of **4a** and **4b** are qualitatively similar. In the $^{31}P\{^1H\}$ NMR spectrum of **4a** two doublets at δ 177.1 and 66.5 ($^2J_{PP}$ = 96.3 Hz) are consistent with a phosphido group bridging two metal atoms and a metal-bound triphenylphosphine, respectively. The magnitude of $^2J_{PP}$ strongly suggests that the phosphido bridge and triphenylphosphine are mutually *trans*. A minor set of doublets (approximately 20%) in the spectrum (δ 176.5 and 63.8, $^2J_{PP}$ = 72.5 Hz) corresponds to an isomer in which the triphenylphosphine is attached to the other iron center (Scheme 1). Similarly, the room-temperature $^{31}P\{^1H\}$ NMR spectrum of **4b** contains two pairs of doublets, one at δ 179.1 and 66.7 ($^2J_{PP}$ = 78.1 Hz) and the other at δ 176.0 and 64.8 ($^2J_{PP}$ = 96.7 Hz), although in contrast to **4a**, these appear as a near-equal mixture of isomers (vide infra). Herein, the two isomers associated with **4a** and **4b** will be referred to as $\mathbf{4a_1}$ and $\mathbf{4a_2}$, and $\mathbf{4b_1}$ and $\mathbf{4b_2}$, respectively. The room-temperature ^1H NMR spectra of **4a** and **4b** contain signals that are also consistent with the presence of two isomers. In the case of **4a**, the two protons attached to C_γ appear as two sets of broad resonances of quite different intensity (5.2:1), a major pair at δ 4.96 and 3.96 and a minor set at δ 4.53 and 3.50, while the methyl groups of **4b** appear as four near-equal-intensity signals (1.2:1) in the region δ 0.05−1.71.

(3) (a) Carty, A. J.; Hogarth, G.; Enright, G.; Frapper, G. *Chem. Commun.* **1997**, 1833. (b) Davies, J. E.; Mays, M. J.; Raithby, P. R.; Sarveswaran, K. *Angew. Chem., Int. Ed. Engl.* **1997**, *36*, 2668.

(4) (a) Chi, Y.; Carty, A. J.; Blenkiron, P.; Delgado, E.; Enright, G. D.; Wang, W.; Peng, S.-M.; Lee, G.-H. *Organometallics* **1996**, *15*, 5269. (b) Delgado, E.; Chi, Y.; Wang, W.; Hogarth, G.; Low, P. J.; Enright, G. D.; Peng, S.-M.; Lee, G.-H.; Carty, A. J. *Organometallics* **1998**, *17*, 2936.

(5) Carty, A. J.; Hogarth, G.; Enright, G. D.; Steed, J. W.; Georganopoulou, D. *Chem. Commun.* **1999**, 1499.

(6) Doherty, S.; Waugh, M.; Scanlan, T. H.; Elsegood, M. R. J.; Clegg, W. *Organometallics* **1999**, *18*, 679.

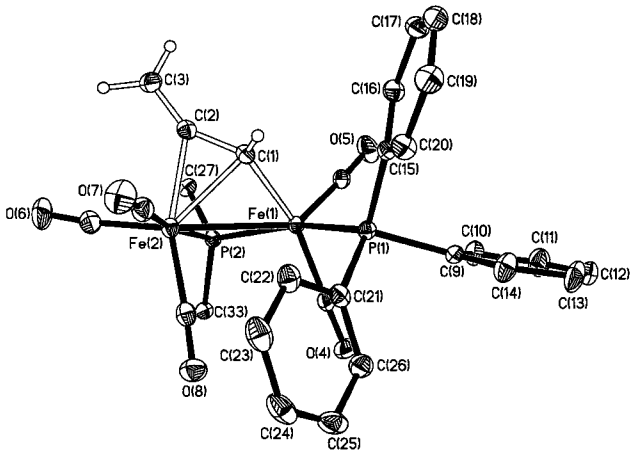

Figure 1. Molecular structure of $[Fe_2(CO)_5(PPh_3)(\mu\text{-}PPh_2)\text{-}\{\mu\text{-}\eta^1\text{:}\eta^2{}_{\alpha,\beta}\text{-}(H)C_\alpha{=}C_\beta{=}C_\gamma H_2\}]$ (**4a$_1$**). Phosphido phenyl rings and phenyl hydrogen atoms have been omitted. Carbonyl carbons have the same numbers as oxygen atoms. Ellipsoids are at the 40% probability level.

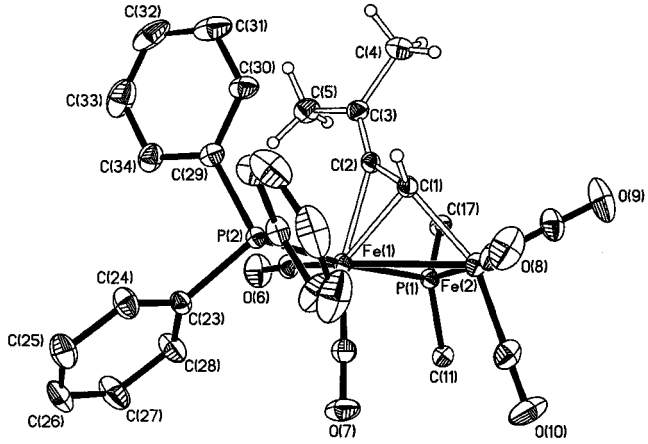

Figure 2. Molecular structure of $[Fe_2(CO)_5(PPh_3)(\mu\text{-}PPh_2)\text{-}\{\mu\text{-}\eta^1\text{:}\eta^2{}_{\alpha,\beta}\text{-}(H)C_\alpha{=}C_\beta{=}C_\gamma Me_2\}]$ (**4b$_2$**). Phosphido phenyl rings and phenyl hydrogen atoms have been omitted. Carbonyl carbons have the same numbers as oxygen atoms. Ellipsoids are at the 40% probability level.

This line broadening is most likely due to a windshield-wiper type motion of the bridging hydrocarbyl ligand, a process common to binuclear σ,η-alkenyl[7] -alkynyl,[8] and -allenyl[9] complexes (vide infra). The $^{13}C\{^1H\}$ NMR spectrum of **4b** contains two sets of three signals at δ 172.6, 133.5, and 109.9 and at δ 177.5, 134.4, and 113.6, which correspond to C_β, C_α, and C_γ of the allenyl fragments in the two isomers. We have also identified similar sets of resonances at δ 184.6, 135.2, and 93.8 and δ 182.4, 135.7, and 96.9 for **4a**, which correspond to the major and minor isomers, respectively. In each case these signals appear in the range previously reported for σ,η-allenyl complexes coordinated through the $C_\alpha{-}C_\beta$ double bond.[10]

Although the spectroscopic data for **4a$_1$** and **4b$_2$** are fully consistent with the expected binuclear allenyl complexes, bonded in a σ,η-manner through the $C_\alpha{-}C_\beta$ double bond, single-crystal X-ray analyses of both were undertaken to obtain precise details on the nature of the metal−ligand bonding and the regioselectivity of substitution. Perspective views of the molecular structures of **4a$_1$** and **4b$_2$**, together with the atomic numbering schemes, are illustrated in Figures1 and 2, respectively, and a selection of bond lengths and angles for both compounds is listed in Table 1. Since these structures differ in the position of phosphine substitution, both will be discussed. The two iron atoms in **4a$_1$** are separated by a distance of 2.6569(4) Å and bridged asymmetrically by a phosphido ligand (Fe(1)−P(2) = 2.2010(6) Å, Fe(2)−P(2) = 2.2487(6) Å). The structure

Table 1. Selected Bond Distances (Å) and Angles (deg) for 4a$_1$ and 4b$_2$

4a$_1$		**4b$_2$**	
Fe(1)−Fe(2)	2.6569(4)	Fe(1)−Fe(2)	2.6318(6)
Fe(1)−P(2)	2.2010(6)	Fe(1)−P(1)	2.2130(9)
Fe(2)−P(2)	2.2487(6)	Fe(2)−P(1)	2.2183(9)
Fe(1)−P(1)	2.2726(6)	Fe(1)−P(2)	2.2468(9)
Fe(1)−C(1)	1.958(2)	Fe(1)−C(1)	2.094(3)
Fe(2)−C(1)	2.109(2)	Fe(1)−C(2)	2.069(3)
Fe(2)−C(2)	2.067(2)	Fe(2)−C(1)	1.973(3)
C(1)−C(2)	1.371(3)	C(1)−C(2)	1.376(4)
C(2)−C(3)	1.317(3)	C(2)−C(3)	1.322(4)
Fe(1)−P(2)−Fe(2)	73.314(18)	Fe(1)−P(1)−Fe(2)	72.87(3)
Fe(1)−C(1)−C(2)	126.68(16)	Fe(2)−C(1)−C(2)	142.1(2)
Fe(2)−C(1)−C(2)	69.16(12)	Fe(1)−C(1)−C(2)	69.71(17)
Fe(2)−C(2)−C(3)	135.21(18)	Fe(1)−C(2)−C(3)	142.3(3)
P(1)−Fe(1)−P(2)	160.05(2)	P(1)−Fe(1)−P(2)	172.56(3)
P(1)−Fe(1)−Fe(2)	108.827(18)	P(2)−Fe(1)−Fe(2)	120.00(3)
Fe(2)−Fe(1)−P(2)	54.169(16)	Fe(2)−Fe(1)−P(1)	53.66(2)
Fe(1)−Fe(2)−P(2)	52.517(16)	Fe(1)−Fe(2)−P(1)	53.47(2)
C(1)−C(2)−C(3)	152.2(2)	C(1)−C(2)−C(3)	145.9(3)

shows an allenyl ligand σ-bonded to Fe(1) (Fe(1)−C(1) = 1.958(2) Å) and η^2-coordinated to Fe(2) (Fe(2)−C(1) = 2.109(2) Å, Fe(2)−C(2) = 2.067(2) Å). The carbon−carbon bond lengths C(1)−C(2) (1.371(3) Å) and C(2)−C(3) (1.317(3) Å) are significantly different and reflect this bonding mode, the former being consistent with the elongation expected upon coordination to a metal center[11] and the latter being in the range expected for a C=C double bond of an allene. The corresponding bond lengths for **4b$_2$** are similar. The iron−carbon and carbon−carbon bond length pattern is similar to that previously reported for binuclear allenyl complexes of group 8. The angle C(1)−C(2)−C(3) (152.2(2)°) is similar to those previously reported for $[Fe_2(CO)_6(\mu\text{-}PPh_2)\{\mu\text{-}\eta^1\text{:}\eta^2{}_{\alpha,\beta}\text{-}(H)C_\alpha{=}C_\beta{=}C_\gamma H_2\}]$ (153.1(2)°)[10a] and $[Fe_2(CO)_6(\mu\text{-}SBu^t)\{\mu\text{-}\eta^1\text{:}\eta^2\text{-}(H)C{=}C{=}CH_2\}]$ (153.1(2)°).[9a] The dihedral angle of 106° between the planes defined by C(3), H(3A), and H(3B) and C(1), Fe(1), and H(1) is consistent with the distortion from pure metalloallenic character necessary to coordinate to Fe(2) through the $C_\alpha{-}C_\beta$ double bond. While the core structural features of **4a$_1$** and **4b$_2$**, in particular the bond lengths and angles within the

(7) (a) MacLaughlin, S. A.; Doherty, S.; Taylor, N. J.; Carty, A. J. *Organometallics* **1992**, *11*, 4315. (b) Patin, H.; Mignani, G.; Benoit, A.; McGlinchey, M. J. *J. Chem. Soc., Dalton Trans.* **1981**, 1278. (c) Hogarth, G.; Lavender, M. H.; Shukri, K. *J. Organomet. Chem.* **1997**, *527*, 247. (d) Hogarth, G. *J. Organomet. Chem.* **1991**, *407*, 91.

(8) Cherkas, A. A.; Randall, S. M.; MacLaughlin, S. A.; Mott, G. N.; Taylor, N. J.; Carty, A. J. *Organometallics* **1988**, *7*, 969.

(9) (a) Seyferth, D.; Womack, G. B.; Archer, C. M.; Dewan, J. C. *Organometallics* **1989**, *8*, 430. (b) Seyferth, D.; Archer, C. M.; Ruschke, D. P.; Cowie, M.; Hilts, R. W. *Organometallics* **1991**, *10*, 3363. (c) Nucciarone, D.; Taylor, N. J.; Carty, A. J. *Organometallics* **1986**, *5*, 1179.

(10) (a) Doherty, S.; Corrigan, J. F.; Carty, A. J.; Sappa, E. *Adv. Organomet. Chem.* **1995**, *37*, 39. (b) Doherty, S.; Elsegood, M. R. J.; Clegg, W.; Rees, N. H.; Scanlan, T. S.; Waugh, M. *Organometallics* **1997**, *16*, 3221. (c) Carleton, N.; Corrigan, J. F.; Doherty, S.; Pixner, R.; Sun, Y.; Taylor, N. J.; Carty, A. J. *Organometallics* **1994**, *13*, 4179.

(11) Hogarth, G.; Lavender, M. H.; Shukri, K. *Organometallics* **1995**, *14*, 2325.

bridging hydrocarbyl ligand and metal−phosphido and metal−allenyl bridges, are essentially the same, they differ in the site of substitution. In **4a$_1$** the triphenylphosphine is located on the iron atom σ-bonded to the allenyl, Fe(1), and is *trans* to the phosphido bridge (P(2)−Fe(1)−P(1) = 160.05(2)°), while in **4b$_2$** it is located on the iron atom η^2-bonded to the allenyl and similarly *trans* to the phosphido bridge (P(2)−Fe(1)−P(1) = 172.56(3)°).

As **4a** and **4b** are the first examples of phosphine-substituted homobinuclear allenyl complexes, the ligand exchange process was investigated further using variable-temperature ^{1}H NMR and NOESY studies. Since both compounds exhibit qualitatively similar line broadening characteristics within the temperature range 233−383 K, only those of **4a** will be discussed in detail. At low temperature (253 K), the distinct isomers **4a$_1$** and **4a$_2$** are each characterized by pairs of low- and high-field doublets with coupling constants of 96.3 and 72.5 Hz, respectively. As the temperature is raised, broadening occurs and the sets of signals collapse such that at 373 K the spectrum shows a sharp high-field doublet at δ 176.1 and a somewhat broader doublet at δ 65.1, showing quite clearly that the two isomers interconvert. The high-temperature phosphorus−phosphorus coupling constant of 86.4 Hz further reveals that the only fluxional process is that of the allenyl ligand and that the phosphine does not undergo a trigonal twist but, rather, remains *trans* to the phosphido bridge throughout. The variable-temperature ^{1}H NMR study of **4a** is shown in Figure 3. At 233 K, the two isomers are clearly distinguished by resonances at δ 5.41 and 4.40 (**4a$_1$**) and at δ 4.66 and 3.69 (**4a$_2$**) as a 6.5:1 mixture (●, major isomer **4a$_1$**; △, minor isomer **4a$_2$**; *, minor impurity; ◊, **5a**). As the temperature is raised, the ratio of isomers changes such that at 303 K it is nearer to 2.5:1. At higher temperatures these resonances broaden and coalesce such that at 383 K two distinct signals are seen at δ 4.54 and 4.42, indicating that rapid interconversion of isomers **4a$_1$** and **4a$_2$** does not result in exchange of the protons attached to C_γ. After prolonged heating at 383 K, the ^{1}H NMR spectrum contains additional resonances that correspond to the thermolysis product **5a**.

As **4a** is not stable for extended periods at high temperatures (see later), more information concerning the precise exchange process was obtained from magnetization transfer experiments (EXSY). The low-temperature EXSY spectrum of **4a** (Figure 4) clearly shows that the signals at δ 5.41 and 3.69 exchange, as do those at δ 4.39 and 4.66. Exchange rates were extracted from the two-dimensional intensity matrix using the program D2DNMR.[12] The rate of conversion of **4a$_1$** to **4a$_2$** is approximately 14.3 s^{-1} (±0.5 s^{-1}), which equates to a free energy of activation for the process of approximately 15.9 kcal mol^{-1} (±0.2 kcal mol^{-1}). A similar value of 16.1 ± 0.2 kcal mol^{-1} was found for exchange of **4b$_1$** with **4b$_2$**, from variable-temperature ^{1}H NMR measurements. The difference in free energy between **4a$_1$** and **4a$_2$** has also been estimated from the temperature dependence of the equilibrium constant, using variable-temperature ^{1}H NMR studies in the temperature range 233−298 K. A straight-line plot of ln K_{eq} versus 1/T corresponds to a difference in free energy of 1.2 kcal mol^{-1} (5.4 kJ mol^{-1}) between **4a$_1$** and **4a$_2$**.

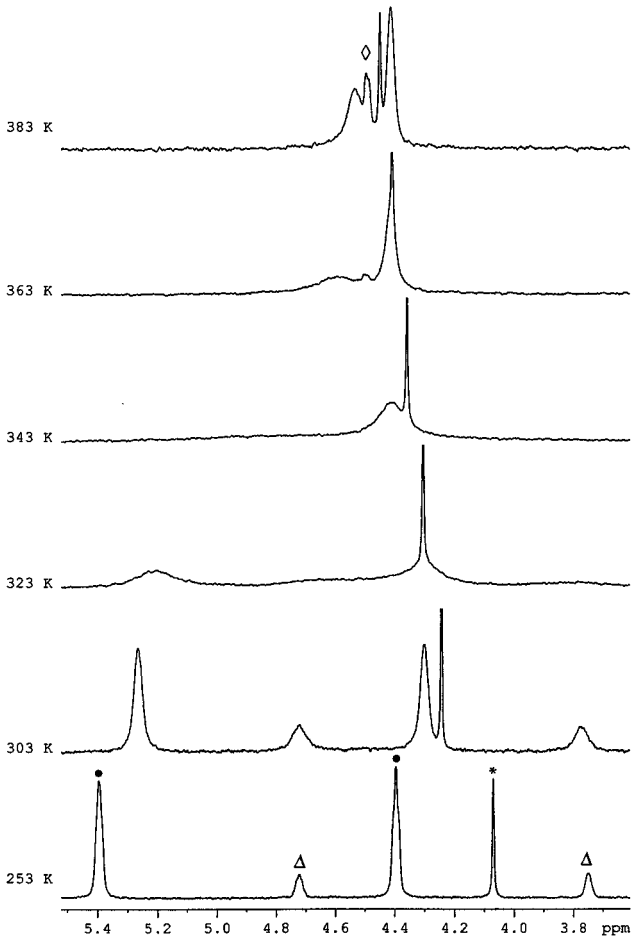

Figure 3. Variable-temperature ^{1}H NMR spectra of [Fe$_2$(CO)$_5$(PPh$_3$)(μ-PPh$_2$){μ-η^1:$\eta^2_{\alpha,\beta}$-(H)C$_\alpha$=C$_\beta$=C$_\gamma$H$_2$}] (**4a**) recorded in d_8-toluene: (●) major isomer **4a$_1$**; (△) minor isomer **4a$_2$**; (*) minor impurity; (◊) **5a**.

The spectroscopic characteristics described above are consistent with a process that interchanges **4a$_1$** and **4a$_2$** via a flipping motion of the σ,η-allenyl group, which involves a perpendicular transition state such as that shown in Figure 5. This mechanism interchanges one isomer, with the triphenylphosphine attached to the σ-bonded iron, with that in which the phosphine is attached to the η^2-bonded iron and is fully consistent with the spectroscopic data. The close similarity between the variable-temperature ^{1}H NMR characteristics and the free energy of activation for **4a** and **4b** suggests that a similar dynamic process is responsible for the line broadening associated with both compounds. This interpretation is supported by the solid-state structures of **4a$_1$** and **4b$_2$**, which correspond to the two proposed substitutional isomers (vide infra). The free energy of activation associated with the windshield-wiper type exchange in **4a** (15.9 kcal mol^{-1}) and **4b** (16.1 kcal mol^{-1}) is higher than that of 13.4 kcal mol^{-1} previously reported for [Fe$_2$(CO)$_6$(μ-PPh$_2$){μ-η^1:$\eta^2_{\alpha,\beta}$-(H)C$_\alpha$=C$_\beta$=C$_\gamma$H$_2$}] (**1a**)[10b] and much closer to the value of 16.1 kcal mol^{-1} for [Fe$_2$(CO)$_4$(μ-dppm)(μ-PPh$_2$)(μ-HC=CH$_2$)].[7d] One plausible explanation for the difference in $\Delta G^\ddagger$ may be the relative strength of the Fe−C$_\beta$ bond, since cleavage of this bond is an integral step to reaching the proposed transition state. The strength of this bond depends on

(12) Abel, E. W.; Coston, T. P. J.; Orrell, K. G.; Sik, V.; Stephenson, D. *J. Magn. Reson.* **1986**, *70*, 34.

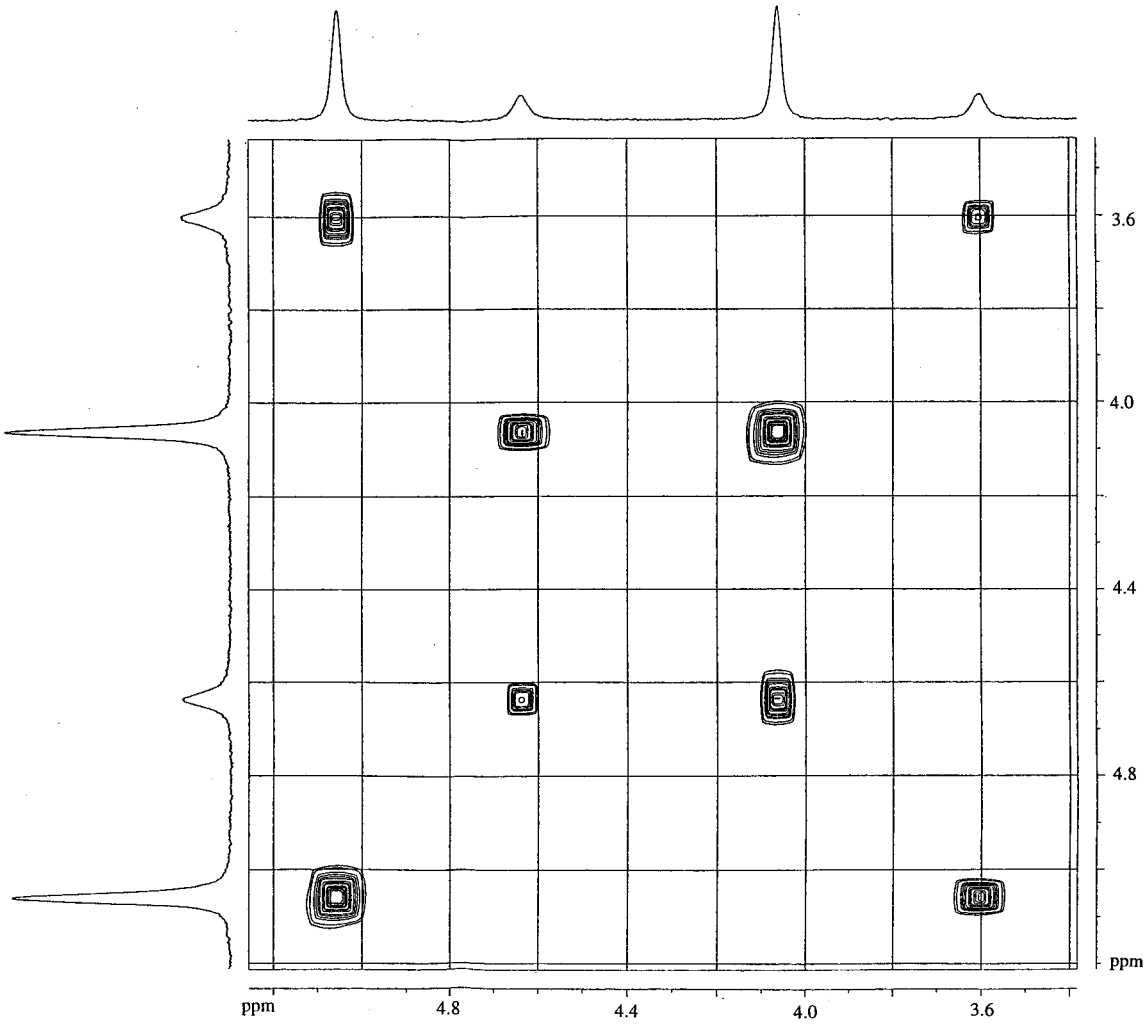

Figure 4. ^{1}H EXSY spectrum of $[Fe_2(CO)_5(PPh_3)(\mu\text{-}PPh_2)\{\mu\text{-}\eta^1\text{:}\eta^2{}_{\alpha,\beta}\text{-}(H)C_\alpha{=}C_\beta{=}C_\gamma H_2\}]$ (**4a**). recorded at 253 K, showing exchange of isomer $\mathbf{4a_1}$ with $\mathbf{4a_2}$.

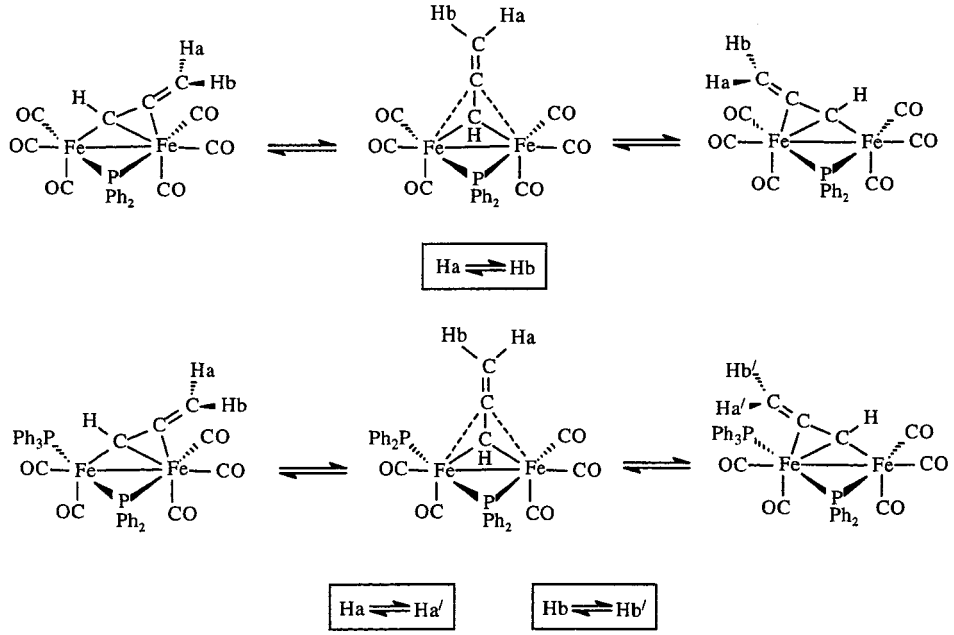

Figure 5. Exchange of σ- and π-allenyl bonding interactions in **1a** and **4a**.

several factors, one of which is the extent of Fe−C π* back-donation, which will be influenced by the substitution of CO for PPh_3.

In an earlier study we proposed that the diastereotopic methylene protons in $[Fe_2(CO)_6(\mu\text{-}PPh_2)\{\mu\text{-}\eta^1\text{:}\eta^2{}_{\alpha,\beta}\text{-}(H)C_\alpha{=}C_\beta{=}C_\gamma H_2\}]$ (**1a**) exchange via a similar

flipping motion which also involved rotation about a carbon−carbon single bond in a zwitterionic transition state.[10b] In fact, exchange of H_a and H_b in **1a** does not require rotation about $C_\beta-C_\gamma$ and can be accounted for solely by the flipping motion shown in Figure 5. Furthermore, the ^{1}H NMR studies described above clearly demonstrate that rotation about $C_\beta-C_\gamma$ in the transition state for exchange of **4a$_1$** with **4a$_2$** does not occur, since this would result in exchange of H_a with H_b and $H_{a'}$ with $H_{b'}$. This revised exchange process also accounts for the exchange of H_a with $H_{a'}$ and of H_b with $H_{b'}$, which is evident in the ^{1}H NOESY spectrum shown in Figure 3.

Carty has considered three possible processes for exchange of the methyl groups in $[Ru_2(CO)_6(\mu\text{-}PPh_2)\{\mu\text{-}\eta^1\text{:}\eta^2_{\beta,\gamma}\text{-}(Ph)C_\alpha{=}C_\beta{=}C_\gamma Me_2\}]$,[9c] one of which involved a flipping motion similar to that shown in Figure 5. This process was eliminated on the basis of variable-temperature $^{13}C\{^1H\}$ NMR studies, which seemed to show that the $Ru(CO)_3$ fragments did not exchange. The favored explanation involved rotation about the exoskeletal bond, via a zwitterionic transition state in which $C_\beta-C_\gamma$ is a single bond, C_β is carbocationic, and the negative charge is delocalized over the $Ru_2P(CO)_6$ framework. Seyferth has reported that the substituents attached to C_γ in thiolate-bridged allenyl derivatives of the type $[Fe_2(CO)_6(\mu\text{-}SBu^t)\{\mu\text{-}\eta^1\text{:}\eta^2\text{-}(R)C{=}C{=}CR'_2\}]$ (R = Et, Bu^t; R′ = H, Me) exchange on the NMR time scale via a flipping motion similar to that described by Figure 5.[9a,b] An approximate free energy of activation for this process of 12.4 kcal mol^{-1} has been calculated using variable-temperature ^{1}H NMR studies and is significantly lower than that calculated for **4a**/**4b**.

Thermolysis of $[Fe_2(CO)_6(\mu\text{-}PPh_2)\{\mu\text{-}\eta^1\text{:}\eta^2\text{-}(H)C_\alpha{=}C_\beta{=}C_\gamma Me_2\}]$ (1b) and $[Fe_2(CO)_5(PPh_3)(\mu\text{-}PPh_2)\{\mu\text{-}\eta^1\text{:}\eta^2\text{-}(H)C_\alpha{=}C_\beta{=}C_\gamma R_2\}]$ (4a,b): Intramolecular Phosphorus−Carbon Bond Formation. Heating a toluene solution of **4a**,**b** at reflux for 16 h resulted in a gradual darkening of the solution and smooth conversion into $[Fe_2(CO)_5(PPh_3)\{\mu\text{-}\eta^1\text{:}\eta^3\text{-}(Ph_2P)HCCCR_2\}]$ (**5a**,**b**) and, in the case of **4a**, $[Fe_2(CO)_4(PPh_3)_2\{\mu\text{-}\eta^1\text{:}\eta^3\text{-}(PPh_2)HCCCH_2\}]$-(**6**), which was separated by column chromatography and characterized by single-crystal X-ray crystallography (eq 1). Two high-field signals in the $^{31}P\{^1H\}$ NMR

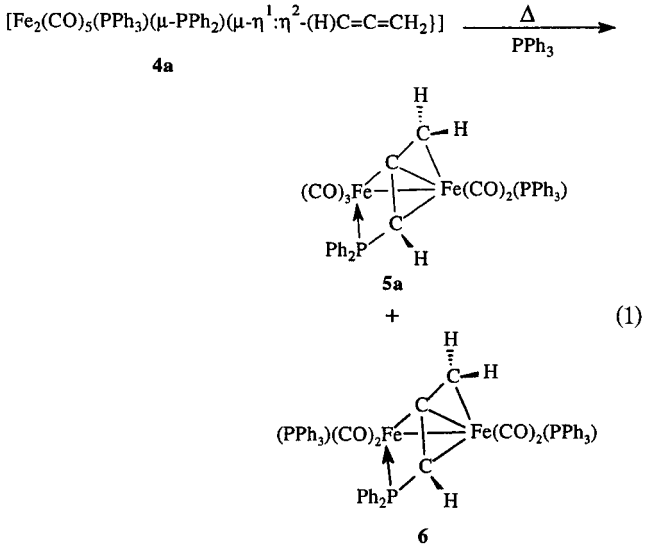

spectrum of **5a** provided the first indication that the phosphido bridge had undergone either phosphorus−carbon bond formation or metal−metal bond cleavage.[13] In the ^{1}H NMR spectrum the two methylene protons attached to C_γ appear as a doublet at δ 4.31 ($^3J_{PH}$ = 4.0 Hz) and a doublet of doublets at δ 2.71 ($^3J_{PH}$ = 13.8 Hz, $^3J_{PH}$ = 4.6 Hz) and the unique proton attached to the PPh_2 substituted carbon gives rise to a doublet of doublets at 2.65 ($^2J_{PH}$ = 16.1 Hz, $^3J_{PH}$ = 3.6 Hz). In the $^{13}C\{^1H\}$ NMR spectrum of **5a** the central carbon of the bridging allyl group appears as a doublet of doublets at δ 183.1 ($^2J_{PC}$ = 46.6 and 3.1 Hz) and the two terminal carbon atoms as doublets of doublets at δ 76.3 ($^2J_{PC}$ = 3.0, $^3J_{PC}$ = 4.1 Hz) and 64.3 ($^1J_{PC}$ = 43.5, $^3J_{PC}$ = 5.2 Hz). The carbonyl region contains two doublets at δ 219.7 and 218.4 and a singlet at δ 211.8, which correspond to the two carbonyls attached to the phosphine-substituted iron atom and the $Fe(CO)_3$ fragment, respectively. The ^{1}H and $^{13}C\{^1H\}$ NMR spectra of **6** are qualitatively similar to those of **5a** in that signals have been identified which clearly correspond to a similar bridging hydrocarbon. The most striking difference between **5a** and **6** lies in their $^{31}P\{^1H\}$ NMR spectra. The former contains two signals, whereas the latter contains three distinct resonances: a singlet at δ 71.1 and doublets at δ 70.2 and 15.1 ($^2J_{PP}$ = 49.0 Hz). The singlet corresponds to the triphenylphosphine attached to the η^3-allyl-bound iron atom, and the two doublets correspond to the PPh_2 group and triphenylphosphine attached to the η^1-bonded iron. The magnitude of $^2J_{PP}$ is consistent with a *cis* arrangement of the PPh_3 and bridging phosphido groups. This assignment implies that **5a**, which contains two singlets in the $^{31}P\{^1H\}$ NMR spectrum, most likely corresponds to the isomer with the triphenylphosphine coordinated to the η^3-bound iron atom, as shown in eq 1. We have shown that refluxing toluene solutions of **5a** do not convert into **6** in the presence of excess triphenylphosphine, which suggests that phosphine substitution most likely occurs prior to phosphorus−carbon bond formation.

In marked contrast to the thermolytic behavior of the parent allenyl complex **1a** (vide infra), a refluxing toluene solution of $[Fe_2(CO)_6(\mu\text{-}PPh_2)\{\mu\text{-}\eta^1\text{:}\eta^2_{\alpha,\beta}\text{-}(H)C_\alpha{=}C_\beta{=}C_\gamma Me_2\}]$ (**1b**) slowly converts into $[Fe_2(CO)_6\{\mu\text{-}\eta^1\text{:}\eta^3\text{-}(Ph_2P)HC_\alpha C_\beta C_\gamma Me_2\}]$ (**7**), identified by the similarity of its $^{31}P\{^1H\}$, ^{1}H, and $^{13}C\{^1H\}$ NMR spectra with those of **5a**,**b** and confirmed by single-crystal X-ray crystallography (eq 2). The $^{31}P\{^1H\}$ NMR spectrum contains a

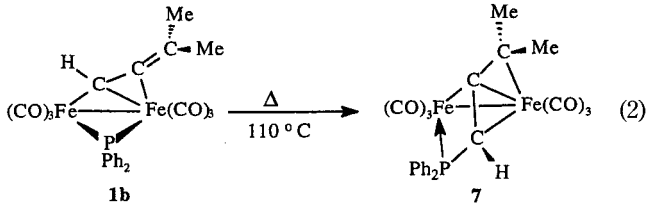

high-field-shifted singlet at δ −18.3, consistent with a transformation involving phosphorus−carbon bond formation. In the ^{1}H NMR spectrum a doublet at δ 3.76 ($^2J_{PH}$ = 2.8 Hz) is assigned to the terminal allylic proton

(13) (a) MacLaughlin, S. A.; Nucciarone, D.; Carty, A. J. In *Phosphorus-31 NMR Spectroscopy in Stereochemical Analysis; Organic Compounds and Metal Complexes*; Verkade, J. G., Quin, L. D., Eds.; VCH, New York, 1987; Chapter 16. (b) Carty, A. J. *Adv. Chem. Ser.* **1982**, *No. 196*, 163.

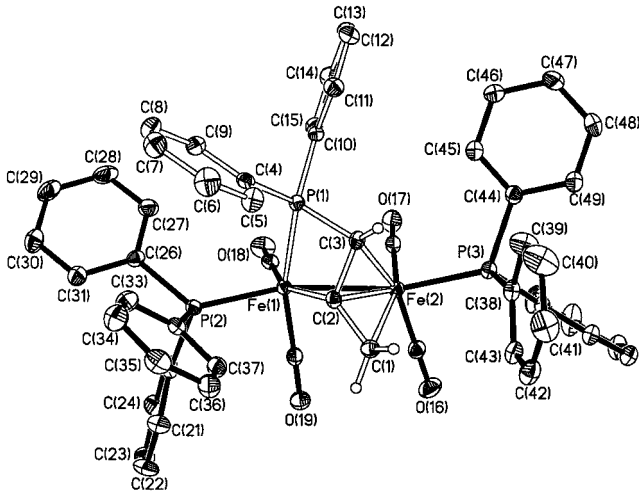

Figure 6. Molecular structure of $[Fe_2(CO)_4(PPh_3)_2\{\mu\text{-}\eta^1\text{:}\eta^3\text{-}(PPh_2)HCCCH_2\}]$ (**6**). Phenyl hydrogen atoms have been omitted. Carbonyl carbons have the same numbers as oxygen atoms. Ellipsoids are at the 40% probability level.

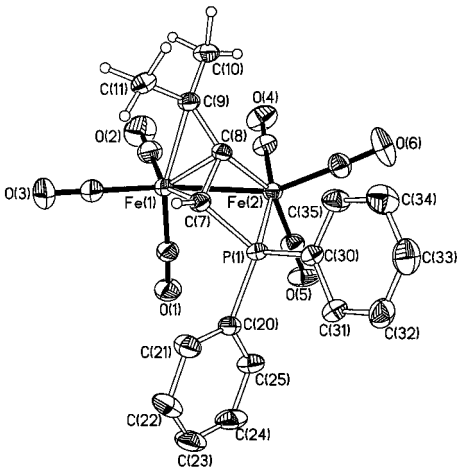

Figure 7. Molecular structure of $[Fe_2(CO)_6\{\mu\text{-}\eta^1\text{:}\eta^3\text{-}(Ph_2P)HCCCMe_2\}]$ (**7**). Phenyl hydrogen atoms have been omitted. Carbonyl carbons have the same numbers as oxygen atoms. Ellipsoids are at the 30% probability level.

and the two methyl groups appear as singlets at δ 2.09 and 1.59. In the $^{13}C\{^1H\}$ NMR spectrum a set of three distinct doublets at δ 167.6 ($^2J_{PC}$ = 32.0 Hz), 118.2 ($^3J_{PC}$ = 24.8 Hz), and 50.8 ($^1J_{PC}$ = 44.5 Hz) belong to the bridging C_3 group and have chemical shifts close to those of the bridging hydrocarbon in **5a**,**b**.

Single-crystal X-ray analyses of **6** and **7** were undertaken to identify the precise nature of the bridging hydrocarbyl ligand and its mode of coordination. Perspective views of the molecular structures of **6** and **7** are shown in Figures 6 and 7, respectively, and a selection of relevant bond lengths and angles for both compounds is listed in Table 2. As expected, formation of **6** and **7** involves regioselective migration of the bridging phosphido group to C_α of the σ,η-allenyl to give a diphenylphosphino-substituted $\sigma\text{-}\eta^3$-allyl, σ-bonded to Fe(1) through the central carbon of the C_3 fragment (Fe(1)−C(2) = 1.979(2) Å) in **6** and η^3-bonded to Fe(2) (Fe(2)−C(1) = 2.163(2) Å, Fe(2)−C(2) = 1.950(2) Å, Fe(2)−C(3) = 2.112(2) Å). The Fe(2)−C(2) bond is considerably shorter than either Fe(2)−C(1) and Fe(2)−C(3) and is comparable to Fe(1)−C(2). In this regard, the bridging

Table 2. Selected Bond Distances (Å) and Angles (deg) for 6 and 7

6		**7**	
Fe(1)−Fe(2)	2.6729(5)	Fe(1)−Fe(2)	2.6227(10)
Fe(1)−P(1)	2.2812(6)	Fe(2)−P(1)	2.2805(11)
Fe(1)−P(2)	2.2241(7)	Fe(2)−C(8)	2.026(3)
Fe(2)−P(3)	2.2397(7)	Fe(1)−C(7)	2.106(4)
Fe(1)−C(2)	1.979(2)	Fe(1)−C(8)	1.961(3)
Fe(2)−C(1)	2.163(2)	Fe(1)−C(9)	2.321(3)
Fe(2)−C(2)	1.950(2)	P(1)−C(7)	1.779(3)
Fe(2)−C(3)	2.112(2)	C(7)−C(8)	1.451(5)
C(3)−P(1)	1.778(2)	C(8)−C(9)	1.399(4)
C(1)−C(2)	1.400(3)		
C(2)−C(3)	1.452(3)		
Fe(2)−Fe(1)−P(2)	159.97(2)	Fe(2)−P(1)−C(7)	82.45(11)
Fe(1)−Fe(2)−P(3)	162.36(2)	Fe(1)−C(7)−P(1)	105.3(2)
Fe(1)−P(1)−C(3)	83.26(8)	Fe(1)−C(8)−C(7)	74.5(2)
Fe(2)−C(3)−P(1)	109.01(11)	Fe(1)−C(8)−Fe(2)	82.24(12)
Fe(2)−C(2)−C(3)	75.14(13)	Fe(1)−C(8)−C(9)	85.6(2)
Fe(1)−C(2)−Fe(2)	85.72(9)	C(7)−C(8)−C(9)	119.4(3)
Fe(1)−C(2)−C(1)	129.59(18)	P(1)−C(7)−C(8)	100.1(2)
C(1)−C(2)−C(3)	117.2(2)	P(1)−Fe(2)−C(8)	70.20(9)
P(1)−C(3)−C(2)	95.85(15)	Fe(2)−C(8)−C(7)	100.6(2)
P(1)−Fe(1)−C(2)	68.37(7)	Fe(1)−C(7)−C(8)	63.8(2)
Fe(1)−C(2)−C(3)	103.97(15)	Fe(1)−C(9)−C(8)	57.4(2)
Fe(2)−C(1)−C(2)	62.08(13)		
Fe(2)−C(2)−C(1)	78.55(14)		

hydrocarbon in **6** may be considered as a μ-alkylidene, flanked by two metalated substituents, CH_2 and CH(PPh_2). This description is supported by the low-field chemical shift of the central carbon atom, which appears at δ 183.1, in the region expected for an alkylidene ligand bridging two iron atoms.[14] The C(1)−C(2) bond distance of 1.400(3) Å is significantly shorter than that of 1.452(3) Å for C(2)−C(3) (Δ = 0.052 Å), which suggests that the former has greater double-bond character and that there is not complete delocalization of the η^3-allylic hydrocarbyl. Similar bond lengths have been reported for related diiron complexes bridged by α-heteroatom functionalized $\sigma\text{-}\eta^3$-allyls, including $[Fe_2(CO)_6(\mu\text{-}\eta^1(C)\text{:}\eta^3(C)\text{:}\eta^1(O)\text{-}Ph_2CCC(Me)OMe\}]$,[15] $[Fe_2(CO)_6\{\mu\text{-}\eta^1(O)\text{:}\eta^3(C)\text{:}\eta^1(S)\text{-}H_2CCC(H)SMe\}]$[16] and $[Fe_2(CO)_6\{\mu\text{-}\eta^1(C)\text{:}\eta^3(C)\text{:}\eta^1(P)\text{-}CC(F)CF_2CF_2C(PR_2)\}]$ (Chart 2).[17] The C(1)−C(2)−C(3) angle of 117.2(2)° is in the range expected for an allyl group η^3-bonded to a single metal center.[18] The phosphorus−carbon bond in the $Ph_2PC(H)CCH_2$ ligand (P(1)−C(3) = 1.778(3) Å) is similar to that in $[Co_2(CO)_6(\mu\text{-}PPh_2)\{\mu\text{-}\eta^1(P)\text{:}\eta^3(C)\text{-}CH_2C(PPh_2)CH_2\}]$ (1.805(11) Å).[19] Both triphenylphosphine ligands lie *transoid* to the Fe−Fe vector (Fe(1)−Fe(2)−P(3) = 162.36(2)°, Fe(2)−Fe(1)−P(2) = 152.97(2)°), and coordination of the α-diphenylphosphino substituent of the

(14) (a) Cherkas, A. A.; Breckenridge, S. M.; Carty, A. J. *Polyhedron* **1992**, *11*, 1075. (b) Hermann, W. A. *Adv. Organomet. Chem*. **1982**, *20*, 159. (c) Hahn, J. E. *Prog. Inorg. Chem*. **1984**, *31*, 205.

(15) (a) Trifonov, L. S.; Orahovats, A. S.; Preow, R.; Heimgartner, H. *Helv. Chim. Acta* **1988**, *71*, 39. (b) Trifonov, L. S.; Orahovats, A. S.; Linden, A.; Heimgartner, H. *Helv. Chim. Acta* **1992**, *75*, 1872. (c) Trifonov, L. S.; Orahovats, A. S.; Heimgartner, H. *Helv. Chim. Acta* **1990**, *73*, 1734.

(16) Seyferth, D.; Ruschke, Davis, W. M.; Cowie, M.; Hunter, A. D. *Organometallics* **1989**, *8*, 836.

(17) Cullen, W. R.; Williams, M.; Einstein, F. W. B.; Willis, A. C. *J. Organomet. Chem*. **1978**, *155*, 259.

(18) (a) Clarke, H. L. *J. Organomet. Chem*. **1974**, *80*, 155. (b) Davis, R. E. *Chem. Commun*. **1968**, 248. (c) Lindley, P. F.; Mills, O. S. *J. Chem. Soc. A* **1970**, 38.

(19) (a) Caffyn, A. J. M.; Mays, M. J.; Solan, G. A.; Conole, G.; Tiripicchio, A. *J. Chem. Soc., Dalton Trans*. **1993**, 2345. (b) Conole, G.; Hill, K. A.; McPartlin, M.; Mays, M. J.; Morris, M. J. *J. Chem. Soc., Dalton Trans*. **1989**, 688.

Chart 1

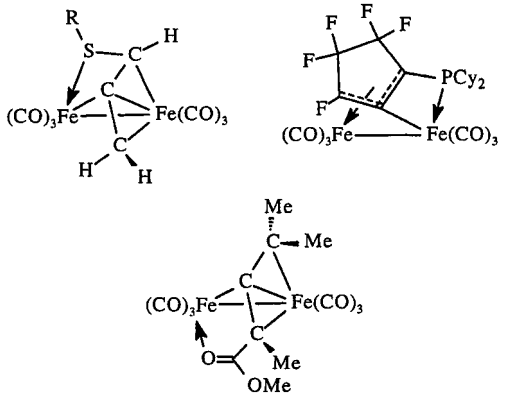

Chart 2

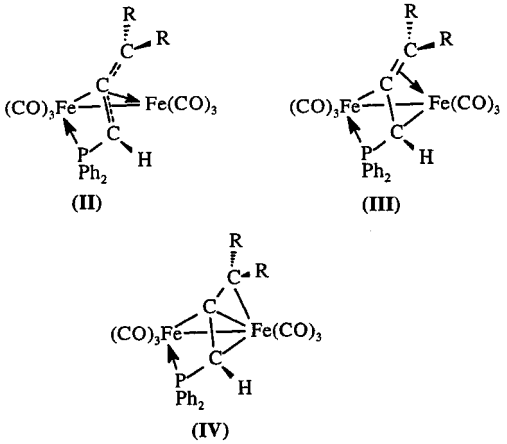

PC_3 chain forms a four-membered metallacycle containing P(1), Fe(1), C(3), and C(2). The solid-state structure of **7** (Figure 7) is qualitatively similar to that of **6** in that it contains a σ,η^3-coordinated diphenylphosphino-substituted allyl, σ-bonded to Fe(2) (Fe(2)−C(8) = 2.026(3) Å) and η^3-bonded to Fe(1) (Fe(1)−C(7) = 2.106(4) Å, Fe(1)−C(8) = 1.961(3) Å, Fe(1)−C(9) 2.321(3) Å). The most striking difference between the structures of **6** and **7** is in the metal−hydrocarbon bonding. In particular, the Fe(1)−C(9) bond length of 2.321(3) Å in **7** (bond type c, Figure 8) is substantially longer than the equivalent Fe(2)−C(1) bond length of 2.163(2) Å in **6** (Δ = 0.158 Å). Although not as marked, the Fe(2)−C(8) bond length of 2.026(3) Å in **7** (bond type d, Figure 8) is also notably longer than its counterpart in **6**. The remaining two Fe−C bond lengths, Fe(1)−C(7) and Fe(1)−C(8) (bond types a and b, Figure 8), are similar to those in **6**.

The series of related σ,η^3-heteroatom coordinated complexes $[Fe_2(CO)_6(\mu\text{-}\eta^1(C):\eta^3(C):\eta^1(O)\text{-}Ph_2CCC(R^1)C(O)OR^2\}]$ have been prepared by irradiation of $[Fe(CO)_5]$ and allene carboxylates.[15] Several have been structurally characterized, and in each case the metal−ligand bonding is qualitatively similar to that found in **6** and **7** in that the iron−carbon bond lengths to the central allylic carbon are significantly shorter than those to the terminal carbons. Further, the two terminal carbon atoms are asymmetrically bonded to iron with a difference of 0.14 Å. As for **7**, the coordination sphere of the η^3-coordinated iron is completed by three carbonyls, while the other contains three carbonyls and the carbonyl oxygen of the ester functionality, which forms a five-membered metallacycle. A comparison of the structures of **6** and **7** with one such complex, $[Fe_2(CO)_6(\mu\text{-}\eta^1(C):\eta^3(C):\eta^1(O)\text{-}Ph_2CCC(Me)C(O)OMe\}]$, shown in Figure 8, illustrates the similarity in the connectivity of the bridging hydrocarbyl fragments.

While the η^3-allyl species **II** adequately describes the connectivity of the bridging hydrocarbon in **6** and **7**, the difference in carbon−carbon (e, f) and iron−carbon (a−c) bond lengths clearly reflects a contribution from the σ,η^2-resonance structure **III**, shown in Chart 2. The similarity in the iron−carbon bond lengths b and d in **6** and **A** also supports a contribution from the alkylidene resonance structure **IV**. Notably, there is a larger than expected variation between the length of the Fe−C bond (c) to the terminal allylic carbon, the largest difference being 0.158 Å.

Overall, **5**−**7** result from a regiospecific 1,2-migration of the phosphido group to the α-carbon atom of the bridging allenyl ligand, possibly to generate a coordinatively unsaturated $\eta^1:\eta^1$-allene bridged intermediate of type **V**, which subsequently binds the pendant olefinic group (Scheme 2). We have found no evidence for 1,3-migration of the phosphido group to the central carbon atom of the allenyl bridge, which would lead to a β-substituted σ,η-allyl group. Such a complex, $[Co_2(CO)_4(\mu\text{-}PPh_2)(\mu\text{-}\eta^1:\eta^1(P):\eta^3(C)\text{-}CH_2C(PPh_2)CH_2)]$, has recently been prepared by the regiospecific insertion of allene into the Co−P bond of $[Co_2(CO)_6(\mu\text{-}PPh_2)_2]$.[19] However, the regiospecificity of the transformation shown in Scheme 2 is perhaps not surprising, since there are a number of examples of addition of phosphorus-based nucleophiles to the α-carbon of the σ,η-allenyl in **1a**.[20]

In a related transformation, $[Ru_2(CO)_6(\mu\text{-}PPh_2)\{\mu\text{-}\eta^1:\eta^2_{\beta,\gamma}\text{-}(Ph)C_\alpha{=}C_\beta{=}C_\gamma H_2\}]$ reacts with dppm to give $[Ru_2(CO)_4(\mu\text{-dppm})\{\mu\text{-}\eta^1:\eta^2\text{-}P(Ph_2)C(O)C(Ph)CCH_2\}]$, which contains a six-electron-donor ketoallenyl phosphine, the product of a coupling sequence involving dual insertion of a carbonyl ligand into the Ru−C_α bond of the C_3-hydrocarbyl ligand and into one arm of the phosphido bridge (eq 3).[10c] There are clear similarities between the

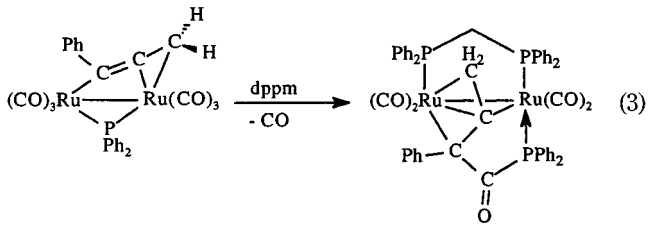

(3)

C_3-bridging fragments in **5**−**7** and $[Ru_2(CO)_4(\mu\text{-dppm})(\mu\text{-}PPh_2)\{\mu\text{-}\eta^1:\eta^2\text{-}P(Ph_2)C(O)C(Ph)CCH_2\}]$, in that both may be considered as α-functionalized $\sigma\text{-}\eta^3$-allyls which also coordinate to a single metal center through a pendant diphenylphosphino group. The most striking difference between these two types of complexes is the presence of a ketonic carbonyl group, which is most likely formed via the allenylcarbonyl intermediate $[Ru_2(CO)_4(\mu\text{-}PPh_2)(\mu\text{-dppm})\{\mu\text{-}\eta^1:\eta^2\text{-}C(O)C(Ph){=}C{=}CH_2\}]$. Although rare, allenylcarbonyl complexes of this type have been reported:[21] for instance, $[Ru_2(CO)_4(\mu\text{-}PPh_2)(\mu\text{-dppm})$-

(20) (a) Doherty, S.; Elsegood, M. R. J.; Clegg, W.; Scanlan, T. H.; Rees, N. H. *Chem. Commun.* **1996**, 1545. (b) Doherty, S.; Elsegood, M. R. J.; Clegg, W.; Ward, M. F. W.; Waugh, M. *Organometallics* **1997**, *16*, 4251. (c) Doherty, S.; Elsegood, M. R. J.; Clegg, W.; Mampe, D. *Organometallics* **1996**, *15*, 5302.

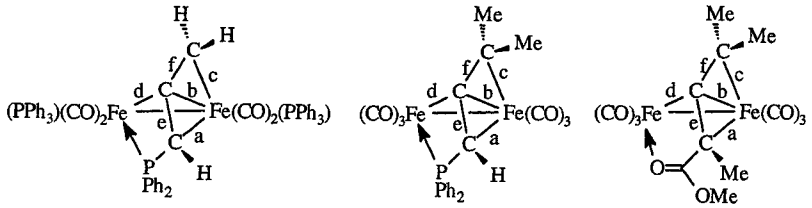

6 **7** **A**

Bond type	6	7	A
a	2.112(2)	2.106(4)	2.133(4)
b	1.950(2)	1.961(3)	1.985(4)
c	2.163(2)	2.321(3)	2.273(4)
d	1.979(2)	2.026(3)	1.987(4)
e	1.452(3)	1.451(5)	1.461(5)
f	1.400(3)	1.399(4)	1.418(5)

Figure 8. Comparison of Fe−C and C−C bond lengths in $[Fe_2(CO)_4(PPh_3)_2\{\mu\text{-}\eta^1\text{:}\eta^3\text{-}(PPh_2)HCCCH_2\}]$ (**6**), $[Fe_2(CO)_6\{\mu\text{-}\eta^1\text{:}\eta^3\text{-}(Ph_2P)HCCCMe_2\}]$ (**7**), and $[Fe_2(CO)_6(\mu\text{-}\eta^1\text{:}\eta^3\text{:}\eta^1\text{-}Ph_2CCC(Me)C(O)OMe\}]$.

Scheme 2

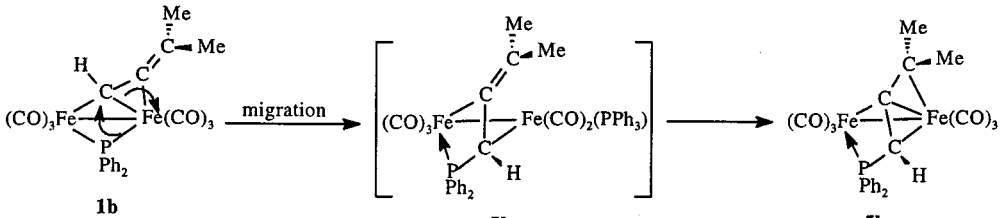

1b **V** **5b**

$\{\mu\text{-}\eta^1\text{:}\eta^2\text{-}C(O)C(Ph)=C=CPh_2\}]$, which easily loses CO to give $[Ru_2(CO)_4(\mu\text{-dppm})(\mu\text{-}PPh_2)\{\mu\text{-}\eta^1\text{:}\eta^2{}_{\alpha,\beta}\text{-}(Ph)C_\alpha=C_\beta=C_\gamma Ph_2]$.[22] In the case of $[Fe_2(CO)_5(PPh_3)(\mu\text{-}PPh_2)\{\mu\text{-}\eta^1\text{:}\eta^2{}_{\alpha,\beta}\text{-}(H)C_\alpha=C_\beta=C_\gamma R_2\}]$ (R = H, Me), migratory insertion of carbon monoxide appears to be less favorable than phosphorus−carbon bond formation.

Thermolysis of $[Fe_2(CO)_6(\mu\text{-}PPh_2)\{\mu\text{-}\eta^1\text{:}\eta^2\text{-}(H)C_\alpha=C_\beta=C_\gamma Me_2\}]$ (1b): Intermolecular Carbon−Carbon Bond Formation. In an attempt to induce coupling of hydrocarbyl units, thermolysis of a toluene solution of the unsubstituted complex $[Fe_2(CO)_6(\mu\text{-}PPh_2)\{\mu\text{-}\eta^1\text{:}\eta^2\text{-}(H)C=C=CH_2\}]$ (**1a**) resulted in the slow formation of $[Fe_4(CO)_{11}(\mu\text{-}PPh_2)_2\{\mu\text{-}\eta^1\text{:}\eta^2\text{:}\eta^1\text{:}\eta^2\text{:}\eta^2\text{-}(H)C=CHCHCHC=CH_2\}]$ (**8**), as an orange-yellow solid. The complex nature of the NMR and IR spectra immediately suggested that **8** was not a binuclear complex, which prompted us to undertake a single-crystal X-ray study to determine the precise nature of this transformation. A perspective view of the molecular structure is shown in Figure 9, together with the atomic numbering scheme, and a selection of bond lengths and angles is listed in Table 3. The most remarkable feature of this structure is the six-carbon chain, formed by coupling of two $\mu\text{-}\eta^1\text{:}\eta^2$-allenyl groups and a 1,2-hydrogen migration. The polycarbon hexa-1,3,5-triene-2,6-diyl ligand is attached to one diiron unit via an alkenyl group, σ-bonded to Fe(4) (Fe(4)−C(17) = 1.986(4) Å) and η^2-bonded to Fe(3) (Fe(3)−C(17) = 2.103-(4) Å, Fe(3)−C(16) = 2.213(4) Å), while the β-substituent of this μ-alkenyl fragment, a butadien-2-yl unit, bridges Fe(1)−Fe(2) via a σ-bond to Fe(1) (Fe(1)−C(15) = 2.180-(4) Å) and two η^2 interactions with C(13)−C(14) (Fe-(1)−C(14) = 2.082(4), Fe(1)−C(13) = 1.928(4) Å) and C(12)−C(13) (Fe(2)−C(12) = 2.167(4) Å, Fe(2)−C(13) = 2.049(4) Å). The C_4 fragment C(12)−C(13)−C(14)−C(15) resembles a $\mu\text{-}\eta^1\text{:}\eta^2\text{:}\eta^2$-coordinated 1,3-butadien-2-yl such as that in $[Fe_2(CO)_5(\mu\text{-}PPh_2)\{\mu\text{-}\eta^2\text{:}\eta^3\text{-}H_2C=C(Me)C=CH_2\}]$ and is reflected in the similarity of the C−C−C angles (143.4(1) vs 143.4(4)° in **8**).[23] The C(12)−C(13) (1.407(6) Å) and C(13)−C(14) (1.406(6) Å) distances are longer than the C=C double bond lengths in butadiene (1.337 Å)[24] and are in the range observed for η^2-alkene and $\eta^1\text{:}\eta^2$-alkenyl complexes of iron.[25] The central C(14)−C(15) bond (1.412(6) Å) is considerably shorter

(21) Wojcicki, A.; Schuchart, C. E. *Coord. Chem. Rev.* **1990**, *105*, 35. (b) Schuchart, C. E.; Young, G. H.; Wojcicki, A.; Calligaris, M.; Nardin, G. *Organometallics* **1990**, *9*, 2417.

(22) Blenkiron, P.; Corrigan, J. F.; Taylor, N. J.; Carty, A. J.; Doherty, S.; Elsegood, M. R. J.; Clegg, W. *Organometallics* **1997**, *16*, 297.

(23) Breckenridge, S. M.; MacLaughlin, S. A.; Taylor, N. J.; Carty, A. J. *J. Chem. Soc., Chem. Commun.* **1991**, 1718.

(24) Almenningen, A.; Bastiansen, O.; Traetteberg, M. *Acta Chem. Scand.* **1958**, *12*, 1211.

(25) (a) Xue, Z.; Sleber, W. J.; Knobler, C. B.; Kaesz, H. D. *J. Am. Chem. Soc.* **1990**, *112*, 1825. (b) Shapley, J. R.; Richter, S. I.; Tacchikawa, M.; Keister, J. B. *J. Organomet. Chem.* **1975**, *94*, C43. (c) Farrugia, L.; Chi, Y.; Tu, W.-C. *Organometallics* **1993**, *12*, 1616. (d) Casey, C. P.; Marder, S. R.; Adams, B. R. *J. Am. Chem. Soc.* **1985,** *107*, 7700.

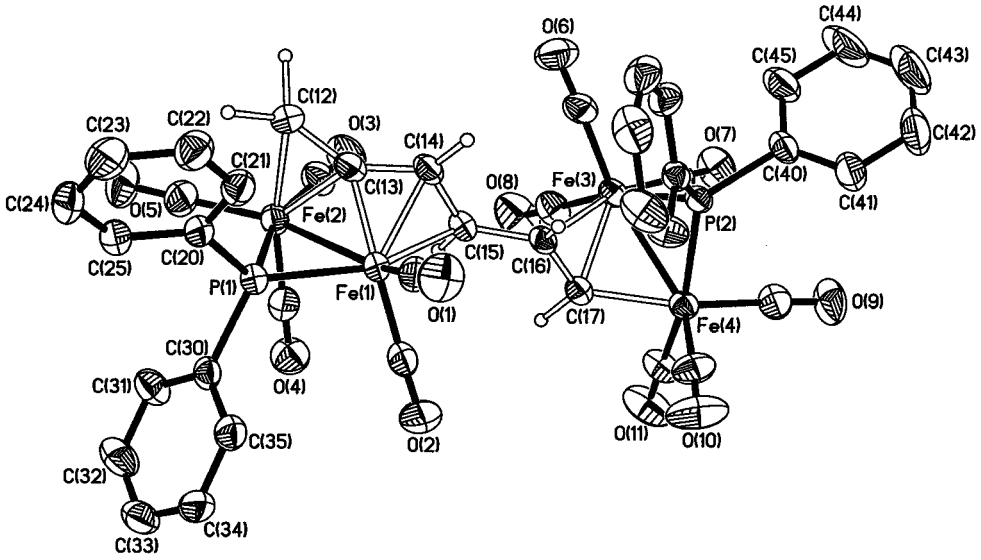

Figure 9. Molecular structure of $[Fe_4(CO)_{11}(\mu\text{-}PPh_2)_2\{\mu\text{-}\eta^1{:}\eta^2{:}\eta^1{:}\eta^2{:}\eta^2\text{-}(H)C{=}CHCHCHC{=}CH_2\}]$ (**8**). Phenyl hydrogen atoms have been omitted. Carbonyl carbons have the same numbers as oxygen atoms. Ellipsoids are at the 30% probability level.

Table 3. Selected Bond Distances (Å) and Angles (deg) for 8

Fe(1)−Fe(2)	2.6444(11)	Fe(1)−P(1)	2.1701(13)
Fe(3)−Fe(4)	2.5974(11)	Fe(2)−P(1)	2.2758(14)
Fe(1)−C(15)	2.180(4)	Fe(3)−P(2)	2.2537(13)
Fe(1)−C(13)	1.928(5)	Fe(4)−P(2)	2.2139(13)
Fe(1)−C(14)	2.082(4)	C(12)−C(13)	1.407(6)
Fe(2)−C(12)	2.167(5)	C(13)−C(14)	1.406(6)
Fe(2)−C(13)	2.049(4)	C(14)−C(15)	1.412(6)
Fe(3)−C(16)	2.213(4)	C(15)−C(16)	1.486(6)
Fe(3)−C(17)	2.103(4)	C(16)−C(17)	1.396(6)
Fe(4)−C(17)	1.986(4)		

Fe(1)−P(1)−Fe(2)	72.95(4)	Fe(4)−C(17)−C(16)	126.3(2)
Fe(3)−P(2)−Fe(4)	71.09(4)	C(12)−C(13)−C(14)	143.4(4)
Fe(1)−C(13)−C(12)	140.3(3)	C(13)−C(14)−C(15)	120.5(4)
Fe(1)−C(13)−C(14)	75.5(3)	C(14)−C(15)−C(16)	118.5(4)
Fe(1)−C(15)−C(14)	66.9(2)	C(15)−C(16)−C(17)	122.8(4)

than in butadiene (1.483 Å) and reflects the delocalized bonding along the polycarbon bridge. Overall, the hexa-1,3,5-triene-2,6-diyl chain functions as a net eight-electron donor, providing five electrons to one binuclear framework and three to the other.

The $^{31}P\{^1H\}$ NMR spectrum of **8** contains two low-field singlets at δ 174.3 and 173.7, which correspond to the two unique bridging phosphido groups. In the ^1H NMR spectrum six distinct, well-separated, nonaromatic protons are clearly visible and are associated with the bridging hexatrienediyl. A low-field doublet of doublets at δ 8.53 ($^3J_{PH}$ = 12.8 Hz, $^3J_{HH}$ = 6.7 Hz) is in the range characteristic of a α-vinyl C−H proton. The two methylene protons attached to the other end of the bridging polycarbon fragment appear as a doublet of doublets at δ 2.78 ($^2J_{HH}$ = 4.9, $^3J_{PH}$ = 11.3 Hz) and a triplet at δ 1.95 ($^3J_{PH}$ = $^2J_{HH}$ = 4.9 Hz). The remaining three internal protons have been assigned to two triplets at δ 5.21 ($^3J_{PH}$ = $^3J_{HH}$ = 5.8 Hz) and 2.98 ($^3J_{HH}$ = $^3J_{HH}$ = 9.1 Hz) and a multiplet at δ 3.59 ($^3J_{HH}$ = 4.6 Hz, $^3J_{HH}$ = 9.5 Hz, $^3J_{HP}$ = 13.8 Hz).

An isotopic labeling experiment provided insight into the regioselectivity of the carbon−carbon coupling step. Heating a toluene solution of $[Fe_2(CO)_6(\mu\text{-}PPh_2)\{\mu\text{-}\eta^1{:}\eta^2\text{-}(D)C_\alpha{=}C_\beta{=}C_\gamma H_2\}]$ (**1a**-*d*) at reflux resulted in the exclusive formation of the single isotopomer $[Fe_4(CO)_{11}(\mu\text{-}PPh_2)_2\{\mu\text{-}\eta^1{:}\eta^2{:}\eta^1{:}\eta^2{:}\eta^2\text{-}(D)C{=}CHCHCDC{=}CH_2\}]$ (**8**-*d*$_2$), identified in the ^2H NMR spectrum by singlets at δ 8.67 and 5.33. This strongly suggests that the proton attached to the α-carbon does not migrate and that **8** results from carbon−carbon coupling between C_γ and C_α (head to tail) of two allenyl groups and 1,2-hydrogen migration from C_γ to C_β, possibly via an intermediate alkenyl such as **VI**, shown in Scheme 3. The formation of **8** can be viewed as addition of the nucleophilic terminal carbon atom of this intermediate to the α-carbon of **1a**, loss of CO, and coordination of the internal double bond of **VII**. In this regard, there is precedent for addition of carbon-based nucleophiles to the α-carbon atom of **1a**.[26] Furthermore, complexes similar to **VI** have been proposed as intermediates in the reaction between alkynes and the cationic bridging methylidyne $[\{Cp_2Fe_2(CO)_2\}(\mu\text{-}CO)(\mu\text{-}CH)]^+$. Electrophilic addition of the methylidyne carbon to the alkyne gives a vinyl-cation-like intermediate or transition state, **VIII**, which is trapped by a terminal carbonyl (Scheme 4).[27] In the case of **VI**, intermolecular coupling to an allenyl group is more favorable than insertion of CO. Conversion of **1b** into **7** (vide supra) lends support to the deuterium labeling experiment in that it indicates that 1,2-hydrogen migration from C_γ to C_β is integral to the formation of the hexa-1,3,5-triene-2,6-diyl. In the case of **1b** there are no protons attached to C_γ and intramolecular phosphorus−carbon bond formation is more favorable than intermolecular carbon−carbon coupling.

Conversion of **1a** into **8** provides the first example of intermolecular coupling of two allenyl groups through C_α and C_γ. Indeed, there are relatively few examples of allenyl−allenyl coupling, the most recent of which involves coupling between C_β and C_γ of the allenyl groups in $[CpRu(CO)_2\{\eta^1\text{-}C(H){=}C{=}CH_2\}]$, in the presence of $[Fe_2(CO)_9]$, to give the mixed iron−ruthenium cluster **B**, which contains an unusual bridging diallyl polycarbon.[28] Other examples of allenyl dimerization

(26) Doherty, S.; Hogarth, G.; Waugh, M.; Scanlan, T. H.; Clegg, W.; Elsegood, M. R. J. *Organometallics* **1999**, *18*, 3178.
(27) Casey, C. P.; Woo, K.; Fagan, P. J.; Palermo, R. E.; Adams, B. R. *Organometallics* **1987**, *6*, 447.
(28) Churchill, M. R.; See, R. F.; Shuchart, C. E.; Wojcicki, A. *J. Organomet. Chem.* **1996**, *512*, 189.

Scheme 3

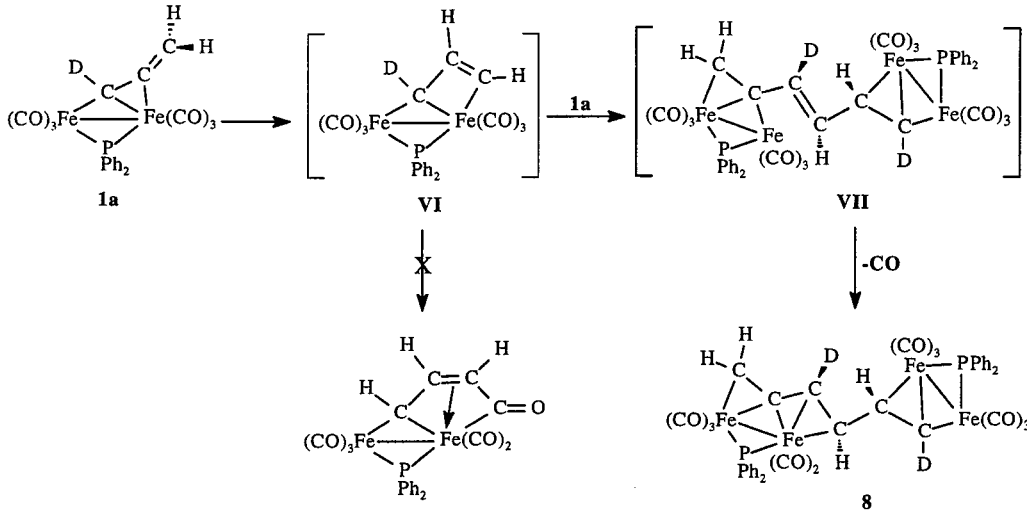

Scheme 4

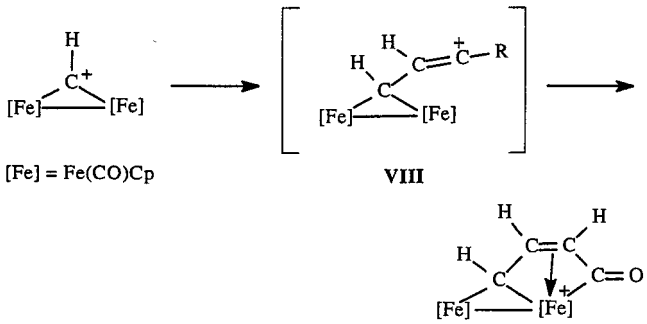

Chart 3

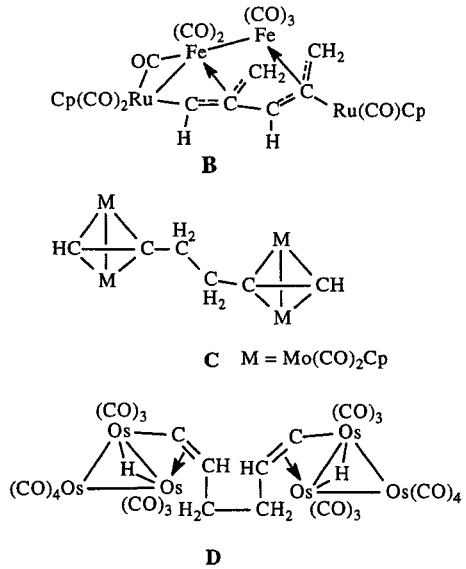

include the redox-promoted coupling of $[\{\eta^5\text{-}C_5H_4Me\}Mo(CO)_2\}_2\{\mu\text{-}\eta^2\text{:}\eta^3\text{-}C(H)CCH_2\}]^+$ to give **C**[29] and the intermolecular reductive coupling of $[CpW(CO)_3\{\eta^1\text{-}C(H)C{=}CH_2\}]$ with $[Os_3H_2(CO)_{10}]$ to give the hexadienediyl-bridged **D** (Chart 3).[30]

The reluctance of **1a** to lose more than one CO and undergo metal−metal bond formation is somewhat surprising, since alkynyl coupling in $[M_2(CO)_6(\mu\text{-}PPh_2)(\mu\text{-}C{\equiv}CR)]$ (M = Fe, Ru) generally results in the loss of several carbonyls. For instance, coupling of the hydrocarbyl in $[Fe_2(CO)_6(\mu\text{-}PPh_2)(\mu\text{-}\eta^1\text{:}\eta^2\text{-}C{\equiv}CPh)]$ is accompanied by the loss of four carbonyls to give $[Fe_4(CO)_8(\mu\text{-}PPh_2)_2(\mu_4\text{-}\eta^1\text{:}\eta^1\text{:}\eta^1\text{:}\eta^1\text{:}\eta^2\text{:}\eta^2\text{:}\eta^2\text{:}\eta^2\text{-}PhCCCCPh)]$.[3] In the case of $[Ru_2(CO)_6(\mu\text{-}PPh_2)(\mu\text{-}\eta^1\text{:}\eta^2\text{-}C{\equiv}CBu^t)]$, metal−metal bond formation precedes coupling of the $\mu\text{-}\eta^1\text{:}\eta^2$-alkynyls to give $[Ru_4(CO)_8(\mu\text{-}PPh_2)(\mu_4\text{-}\eta^1\text{:}\eta^2\text{:}\eta^2\text{:}\eta^1\text{:}\eta^2\text{:}\eta^2\text{-}Bu^t\text{-}CCCCBu^t)]$, via the intermediate bis-alkynyl $[Ru_4(CO)_9(\mu\text{-}PPh_2)_2(\mu\text{-}\eta^1\text{:}\eta^2\text{-}C{\equiv}CBu^t)_2]$.[4]

In summary, the σ,η-allenyl complexes $[Fe_2(CO)_{6-n}(PPh_3)_n(\mu\text{-}PPh_2)\{\mu\text{-}\eta^1\text{:}\eta^2\text{-}(H)C{=}C{=}CR_2\}]$ (n = 0, 1) are generally reluctant to undergo carbon−carbon coupling to generate new polycarbon structures. In the majority of cases the dominant reaction pathway is 1,2-migration of the bridging phosphido group to the α-carbon of the σ,η-allenyl fragment to give a diphenylphosphino-substituted allyl which bridges the two iron atoms in a σ,η^3-manner. In contrast, thermolysis of the parent allenyl complex **1a** resulted in carbon−carbon coupling of two allenyl groups to give an unusual eight-electron-donor hexa-1,3,5-triene-2,6-diyl. It appears that substitution of phosphine for CO favors 1,2-migration of the phosphido bridge over carbon−carbon coupling, as does the absence of protons attached to C_γ. This is perhaps not surprising, since both CO substitution and 1,2-hydrogen migration, from C_γ to C_β, are integral to this process. These studies further broaden the reactivity of σ,η-allenyl diiron complexes[31] and suggest that it may be possible to construct multimetallic arrays bridged by more elaborate organic architectures by extending the intermolecular coupling reactions to α-functionalized σ,η-allenyl complexes.

Experimental Section

General Procedures. Unless otherwise stated, all manipulations were carried out in an inert-atmosphere glovebox or by using standard Schlenk line techniques. Diethyl ether and hexane were distilled from Na/K alloy, tetrahydrofuran

(29) Meyer, A.; McCabe, D. J.; Curtis, M. D. *Organometallics* **1987**, *6*, 1491.

(30) Chen, M.-C.; Keng, R.-S.; Lin, Y.-C.; Wang, Y.; Cheng, M.-C.; Lee, G.-H. *J. Chem. Soc., Chem. Commun.* **1990**, 1138.

(31) (a) Doherty, S.; Hogarth, G.; Elsegood, M. R. J.; Clegg, W.; Rees, N. H.; Waugh, M. *Organometallics* **1998**, *17*, 3331. (b) Doherty, S.; Elsegood, M. R. J.; Clegg, W.; Waugh, M. *Organometallics* **1996**, *15*, 2688. (c) Doherty, S.; Elsegood, M. R. J.; Clegg, W.; Mampe, D. *Organometallics* **1997**, *16*, 1186.

was distilled from potassium, and dichloromethane was distilled from CaH_2. $CDCl_3$ was predried with CaH_2, vacuum-transferred, and stored over 4 Å molecular sieves. ^1H and ^{31}P NMR spectra were recorded on a JEOL LAMBDA 500 instrument or Bruker AC 200, AMX 300, and DRX 500 machines. Hydrogen-1 two-dimensional exchange (EXSY) spectra were obtained using the Bruker automation program NOESYTP. Variable mixing times were utilized between 10 ms and 1 s. Exchange rates for **4b** were calculated from a spectrum with a 20 ms mixing time and extracted from the resulting two-dimensional intensity matrix using the program D2DNMR.[12] Reactions were monitored by thin-layer chromatography (Baker Flex silica gel, 1B-F). Column chromatography was carried out with alumina purchased from Aldrich Chemical Co. and deactivated with 6% w/w water prior to loading. The diiron complexes $[Fe_2(CO)_6(\mu\text{-}PPh_2)\{\mu\text{-}\eta^1{:}\eta^2\text{-}(H)C{=}C{=}CR_2\}]$ (**1a**,**b**) were prepared according to previously published procedures.[10b]

Preparation of $[Fe_2(CO)_5(\mu\text{-}PPh_2)(PPh_3)\{\mu\text{-}\eta^1{:}\eta^2\text{-}(H)C{=}C{=}CH_2\}]$ (4a). A toluene solution of $[Fe_2(CO)_6(\mu\text{-}PPh_2)\{\mu\text{-}\eta^1{:}\eta^2\text{-}(H)C{=}C{=}CH_2\}]$ (**1a**; 0.200 g, 0.4 mmol) and triphenylphosphine (0.104 g, 0.4 mmol) was heated at reflux for 2 h, after which time the solvent was removed in vacuo. The residue was extracted into dichloromethane (2−3 mL), absorbed onto deactivated alumina, desolvated, and placed on a 300 × 30 mm alumina column, which was eluted with an *n*-hexane/dichloromethane mixture (80:20, v/v) to give a single major band identified as **4a**. Crystallization from dichloromethane/methanol gave **4a** as orange crystals in 60% yield (0.177 g). IR (ν(CO), cm^{-1}, C_6H_{14}): 2040 s, 1994 s, 1984 s, 1961 w, 1928 w. $^{31}P\{^1H\}$ NMR (121.5 MHz, $CDCl_3$, δ): 177.1 (d, $^2J_{PP} = 96.3$ Hz, PPh_2, **4a₁**), 176.5 (d, $^2J_{PP} = 72.5$ Hz, PPh_2, **4a₂**), 66.5 (d, $^2J_{PP} = 96.3$ Hz, PPh_3, **4a₁**), 63.8 (d, $^2J_{PP} = 72.5$ Hz, PPh_3, **4a₂**).^1H NMR (500.1 MHz, $CDCl_3$, 258 K, δ): 7.71 (d, $^3J_{PH} = 8.2$, 1H, **4a₂**), 7.44 (d, $^3J_{PH} = 9.75$, 1H, **4a₁**), 7.69−6.99 (m, 25H, C_6H_5), 7.44 (br s, 1H, C(*H*)=C=CH_2), 4.96 (br s, 1H, C=C=CH_aH$_b$, **4a₁**), 4.53 (br s, 1H, C=C=CH_a*H$_b$*, **4a₂**) 3.96 (br s, 1H, C=C=CH_a*H$_b$*, **4a₁**), 3.37 (br s, C=C=CH_a*H$_b$*, **4a₂**). $^{13}C\{^1H\}$ NMR (125.65 MHz, $CDCl_3$, δ): 218.7 (t, $^2J_{PC} = 16.0$ Hz, *C*O), 218.1 (br, *C*O), 214.4 (m, *C*O), 212.5 (t, $^2J_{PC} = 17.4$ Hz, *C*O), 211.4 (br, *C*O), 184.6 (s, C=*C*=CH_2, **4a₁**), 182.4 (s, C=*C*=CH_2, **4a₂**), 140.9−127.0 (m, C_6H_5), 135.7 (d, $J_{PC} = 39.3$ Hz, *C*H=C=CH_2, **4a₂**), 135.2 (d, $J_{PC} = 30.1$ Hz, *C*H=C=CH_2, **4a₁**) 96.9 (s, C=C=*C*H$_2$, **4a₂**), 93.8 (s, C=C=*C*H$_2$, **4a₁**). Anal. Calcd for $C_{38}H_{28}Fe_2O_5P_2$: C, 61.82; H, 3.82. Found: C; 61.43; H, 3.61.

Preparation of $[Fe_2(CO)_5(\mu\text{-}PPh_2)(PPh_3)\{\mu\text{-}\eta^1{:}\eta^2\text{-}(H)C{=}C{=}CMe_2\}]$ (4b). Compound **4b** was prepared using a procedure similar to that described above for **4a** and was obtained as orange crystals in 80% yield from dichloromethane/methanol at room temperature. IR (ν(CO), cm^{-1}, C_6H_{14}): 2040 s, 1994 s, 1984 s, 1961 w, 1928 w. $^{31}P\{^1H\}$ NMR (202.35 MHz, $CDCl_3$, δ): 179.1 (d, $^2J_{PP} = 78.1$ Hz, PPh_2, **4b₂**), 176.0 (d, $^2J_{PP} = 96.7$ Hz, PPh_2, **4b₁**), 66.7 (d, $^2J_{PP} = 96.7$ Hz, PPh_3, **4b₁**), 64.8 (d, $^2J_{PP} = 78.1$ Hz, PPh_3, **4b₂**). ^1H NMR (500.1 MHz, $CDCl_3$, δ): 7.70−6.28 (m, 25H, C_6H_5), 7.06 (d, $^3J_{PH} = 6.1$ Hz, 1H, C{*H*}=C=CMe_2, **4b₂**), 7.01 (d, $^3J_{PH} = 6.4$ Hz, 1H, C{*H*}=C=CMe_2), 1.71 (br s, 3H, *Me*, **4b₁**), 1.29 (br, s, 3H, *Me*, **4b₂**), 0.86 (s, 3H, *Me*, **4b₁**), 0.05 (br s, 3H, *Me*, **4b₂**). $^{13}C\{^1H\}$ NMR (125.65 MHz, $CDCl_3$, δ): 219.7 (t, $^2J_{PC} = {}^2J_{PC} = 18.6$ Hz, *C*O), 219.0 (t, $^2J_{PC} = {}^2J_{PC} = 15.5$ Hz, *C*O), 218.5 (dd, $^3J_{PC} = 12.4$ Hz, $^2J_{PC} = 26.9$ Hz, *C*O), 215.8 (m, *C*O), 211.6 (dd, $^2J_{PC} = 19.7$ Hz, $^3J_{PC} = 15.5$ Hz, *C*O), 177.7 (d, $^2J_{PC} = 8.3$ Hz, C=*C*=CMe_2, **4b₂**), 172.6 (d, $^2J_{PC} = 5.2$ Hz, C=*C*=CMe_2, **4b₁**), 140.4−125.9 (m, C_6H_5), 134.4 (d, $J_{PC} = 39.7$ Hz, *C*=C=CMe_2, **4b₂**), 133.5 (d, $J_{PC} = 31.8$ Hz, *C*=C=CMe_2, **4b₁**), 113.6 (s, C=C=*C*Me_2, **4b₂**), 109.9 (d, $^3J_{PC} = 3.1$ Hz, C=C=*C*Me_2, **4b₁**), 29.8 (s, *Me*, **4b₁**), 29.3 (s, *Me*, **4b₂**), 21.8 (s, *Me*, **4b₁**), 19.9 (s, *Me*, **4b₂**). Anal. Calcd for $C_{40}H_{32}Fe_2O_5P_2$: C, 62.69; H, 4.21. Found: C; 62.43; H, 4.11.

Preparation of $[Fe_2(CO)_5(PPh_3)\{\mu\text{-}\eta^1{:}\eta^3{:}\eta^1(P)\text{-}(Ph_2P)HCCCH_2\}]$ (5a) and $[Fe_2(CO)_4(PPh_3)_2\{\mu\text{-}\eta^1{:}\eta^3{:}\eta^1(P)\text{-}(Ph_2P)HCCCH_2\}]$ (6). A toluene solution of $[Fe_2(CO)_5(\mu\text{-}PPh_2)(PPh_3)\{\mu\text{-}\eta^1{:}\eta^2\text{-}(H)C{=}C{=}CH_2\}]$ (**4a**; 0.200 g, 0.271 mmol) was heated at reflux for 8 h until all the starting material had been consumed. The solution was cooled to room temperature and the solvent removed under reduced pressure to leave a gummy amber residue. The residue was extracted into dichloromethane (2−3 mL), absorbed onto deactivated alumina, desolvated, and placed on a 300 × 30 mm alumina column and eluted with *n*-hexane/dichloromethane (70:30, v/v) to give two well-separated bands, the first identified as **5a** and the second as **6**. The first band was crystallized from *n*-hexane to give **5a** as orange crystals in 50% yield (0.136 g). The second was crystallized from dichloromethane/methanol to give red crystals of **6** in 20% yield (0.053 g).

Compound 5a. IR (ν(CO), cm^{-1}, C_6H_{14}): 2038 s, 1979 s, 1957 w, 1930 w. $^{31}P\{^1H\}$ NMR (121.5 MHz, $CDCl_3$, δ): 70.6 (s, PPh_3), −4.9 (s, PPh_2). ^1H NMR (500.1 MHz, $CDCl_3$, δ): 7.65−6.64 (m, 25H, C_6H_5), 4.41 (d, $^3J_{PH} = 4.0$ Hz, 1H, (PPh_2)-HCCCH_aH$_b$), 2.71 (dd, $^3J_{PH} = 13.8$ Hz, $^3J_{PH} = 4.6$ Hz, 1H, (PPh_2)HCCCH$_a$*H$_b$*), 2.65 (dd, $^2J_{PH} = 16.2$ Hz, $^3J_{PH} = 3.6$ Hz, 1H, (PPh_2)*H*CCCH$_a$H$_b$). $^{13}C\{^1H\}$ NMR (125.65 MHz, $C_6D_5CD_3$, δ): 219.7 (dd, $^2J_{PC} = 12.4$ Hz, $^3J_{PC} = 2.1$ Hz, *C*O), 218.4 (d, $^3J_{PC} = 2.0$ Hz, *C*O), 211.8 (s, *C*O), 183.1 (dd, $^2J_{PC} = 46.6$ Hz, $^2J_{PC} = 3.1$ Hz, (PPh_2)HC*C*CH$_a$H$_b$), 139.5−123.4 (m, C_6H_5), 76.3 (dd, $^2J_{PC} = 30.0$ Hz, $^3J_{PC} = 4.1$ Hz, (PPh_2)HCC*C*H$_a$H$_b$), 64.3 (dd, $^1J_{PC} = 43.5$ Hz, $^2J_{PC} = 5.2$ Hz, (PPh_2)HCCCH$_a$H$_b$). Anal. Calcd for $C_{38}H_{28}Fe_2O_5P_2$: C, 61.82; H, 3.82. Found: C; 61.57; H, 3.66.

Compound 6. IR (ν(CO), cm^{-1}, C_6H_{14}): 1996 s, 1963 m, 1952 m, 1913 w. $^{31}P\{^1H\}$ NMR (121.5 MHz, $CDCl_3$, δ): 71.1 (s, PPh_3), 70.2 (d, $^2J_{PP} = 49.0$ Hz, PPh_3), −15.1 (d, $^2J_{PP} = 49.0$ Hz, PPh_2). ^1H NMR (500.1 MHz, $CDCl_3$, δ): 7.58−6.49 (m, 40H, C_6H_5), 4.35 (br s, 1H, (PPh_2)HCCCH_aH$_b$), 2.63 (s, 1H, (PPh_2)HCCCH$_a$*H$_b$*), 2.60 (s, 1H, (PPh_2)*H*CCCH$_a$H$_b$). $^{13}C\{^1H\}$ NMR (125.65 MHz, $CDCl_3$, δ): 221.4 (d, $^2J_{PC} = 11.8$ Hz, *C*O), 179.6 (d, $^2J_{PC} = 46.7$ Hz, (PPh_2)HC*C*CH$_2$), 140.0−126.9 (m, C_6H_5), 76.3 (d, $^2J_{PC} = 30.9$ Hz, (PPh_2)HCC*C*H$_2$), 65.8 (dd, $^1J_{PC} = 42.7$ Hz, $^2J_{PC} = 4.2$ Hz, (PPh_2)HCCCH$_2$). Anal. Calcd for $C_{55}H_{43}Fe_2O_4P_3$. C, 67.92; H, 4.46. Found: C, 68.11; H, 4.44.

Preparation of $[Fe_2(CO)_5(PPh_3)\{\mu\text{-}\eta^1{:}\eta^3{:}\eta^1(P)\text{-}(Me_2)CCCH(PPh_2)\}]$ (5b). A toluene solution of $[Fe_2(CO)_5(\mu\text{-}PPh_2)(PPh_3)\{\mu\text{-}\eta^1{:}\eta^2\text{-}(H)C{=}C{=}CH_2\}]$ (**4a**; 0.200 g, 0.261 mmol) was heated at reflux for 8 h until all the starting material had been consumed. The solution was cooled to room temperature and the solvent removed under reduced pressure to leave a gummy amber residue. This was extracted into dichloromethane (2−3 mL), absorbed onto deactivated alumina, desolvated, and placed on a 300 × 30 mm alumina column and eluted with *n*-hexane/dichloromethane (70:30, v/v) to give a single major product, identified as **5b**. Crystallization from *n*-hexane/dichloromethane gave orange-red crystals of **5b** in 60% yield (0.120 g). IR (ν(CO), cm^{-1}, C_6H_{14}): 2033 s, 1973 s, 1934 w. $^{31}P\{^1H\}$ NMR (121.498 MHz, $CDCl_3$, δ): 82.2 (s, PPh_3), −9.7 (s, PPh_2). ^1H NMR (500.1 MHz, $CDCl_3$, δ): 7.62−6.63 (m, 25H, C_6H_5), 3.75 (d, $^3J_{PH} = 3.3$ Hz, 1H, (Ph_2P)*H*CCCMe$_a$Me$_b$), 2.00 (s, 3H, (Ph_2P)HCCC*Me$_a$*Me$_b$), 1.66 (s, 3H, (Ph_2P)HCCCMe$_a$*Me$_b$*). Anal. Calcd for $C_{40}H_{32}Fe_2O_5P_2$: C, 62.66; H, 4.21. Found: C; 62.36; H, 3.81.

Preparation of $[Fe_2(CO)_6\{\mu\text{-}\eta^1{:}\eta^3{:}\eta^1(P)\text{-}(Ph_2P)HCCCMe_2\}]$ (7). Heating a toluene solution of $[Fe_2(CO)_6(\mu\text{-}PPh_2)\{\mu\text{-}\eta^1{:}\eta^2\text{-}(H)C{=}C{=}CMe_2\}]$ (**1b**; 0.2 0 g, 0.376 mmol) at reflux for 3 h resulted in a gradual color change from red to amber. The reaction mixture was cooled to room temperature and the solvent removed in vacuo. The residue was extracted in to the minimum volume of dichloromethane (2−3 mL), absorbed onto deactivated alumina, desolvated, and placed on a 300 × 30 mm column and eluted with *n*-hexane to give a single major band identified as **7**. Concentration of the collected fraction and subsequent cooling to −20 °C afforded orange crystals of **7** in 80% yield (0.160 g). IR (ν(CO), cm^{-1}, C_6H_{14}): 2056 m, 2015 s, 1984 s, 1979 s, 1963 w. $^{31}P\{^1H\}$ NMR (121.5 MHz, $CDCl_3$, δ): −18.3 (s, PPh_2). ^1H NMR (500.1 MHz, $CDCl_3$, δ): 7.99−7.18 (m, 10H, C_6H_5), 3.76 (d, $^2J_{PH} = 2.8$ Hz, 1H, (Ph_2P)-

Table 4. Summary of Crystal Data and Structure Determination for Compounds 4a$_1$, 4b$_2$, and 6−8

	4a$_1$	**4b$_2$**	**6**·CH_2Cl_2	**7**	**8**
mol formula	$C_{38}H_{28}Fe_2O_5P_2$	$C_{41}H_{38}Fe_2O_6P_2$	$C_{55}H_{43}Fe_2O_4P_3.CH_2Cl_2$	$C_{23}H_{17}Fe_2O_6P$	$C_{42}H_{26}Fe_4O_{12}P_2$
fw	738.24	800.35	1057.43	532.04	1007.97
cryst size, mm	0.63 × 0.17 × 0.05	0.80 × 0.14 × 0.10	0.50 × 0.32 × 0.28	0.36 × 0.30 × 0.12	0.46 × 0.30 × 0.26
temp, K	160(2)	160(2)	160(2)	293(2)	293(2)
cryst syst	triclinic	monoclinic	triclinic	monoclinic	monoclinic
space group	$P\bar{1}$	$P2_1/n$	$P\bar{1}$	$P2_1/c$	$P2/n$
a, Å	10.3058(7)	11.4972(10)	12.1511(8)	15.678(3)	8.762(2)
b, Å	11.5096(8)	17.8548(15)	13.0698(9)	8.167(2)	33.493(7)
c, Å	15.2599(11)	18.5580(16)	17.2688(11)	18.313(4)	14.624(3)
α, deg	74.117(2)		74.938(2)		
β, deg	75.458(2)	102.970(2)	85.383(2)	94.94(3)	94.12(3)
γ, deg	72.393(2)		68.655(2)		
V, Å^3	1631.2(2)	3712.4(6)	2466.3(3)	2336.1(9)	4281(2)
Z	2	4	2	4	4
D_{calcd}, g cm^{-3}	1.503	1.432	1.424	1.513	1.564
μ, mm^{-1}	1.032	0.915	0.841	1.346	1.464
F(000)	756	1656	1088	1080	2032
θ range, deg	2.11−29.02	1.91−28.77	1.73−28.79	2.61−25.06	2.63−22.53
max indices: *h*, *k*, *l*	13, 15, 20	14, 23, 24	16, 17, 23	18, 9, 21	9, 36, 15
no. of rflns measd	13 551	22 624	21 763	4249	11 777
no. of unique rflns	7724	8817	11 444	4093	5615
no. of rflns with $F^2 > 2\sigma(F^2)$	5413	5937	8603	3081	4115
transmissn coeff range	0.563−0.950	0.528−0.914	0.679−0.799	0.791−0.975	
R_{int} (on F^2)	0.0266	0.0432	0.0213	0.0270	0.0570
weighting params[a] *a*, *b*	0.0363, 0.000	0.0791, 0.000	0.0670, 0.000	0.0434, 1.5444	0.0487, 0.4487
R[b]	0.0333	0.0474	0.0417	0.0379	0.0370
R_w[c]	0.0700	0.1348	0.1106	0.1005	0.1068
no. of params	433	469	613	289	523
GOF[d] on F^2	0.881	0.979	1.016	1.039	1.062
max, min diff map, e Å^{-3}	0.411, −0.356	1.403, −0.701	0.985, −1.180	0.289, −0.295	0.413, −0.368

[a] $w^{-1} = \sigma^2(F_o^2) + (aP)^2 + bP$, where $P = (F_o^2 + 2F_c^2)/3$. [b] Conventional $R = \sum||F_o| - |F_c||/\sum|F_o|$ for "observed" reflections having $F_o^2 > 2\sigma(F_o^2)$. [c] $R_w = [\sum w(F_o^2 - F_c^2)^2/\sum w(F_o^2)^2]^{1/2}$ for all data [d] GOF = $[\sum w(F_o^2 - F_c^2)^2/((\text{no. of unique reflections}) - (\text{no. of parameters}))]^{1/2}$.

*H*CCCMe$_2$), 2.65 (s, 3H, (Ph$_2$P)HCCCMe$_a$*Me$_b$*), 2.09 (s, 3H, (Ph$_2$P)HCCC*Me$_a$*Me$_b$). ^{13}C{^{1}H} NMR (125.65 MHz, $CDCl_3$, *δ*): 213.1 (s, CO), 211.9 (s, CO), 167.6 (d, $^2J_{PC}$ = 32.0 Hz, (Ph$_2$P)-HC*C*CMe$_2$), 138.1−128.6 (m, *C*$_6$H$_5$), 118.2 (d, $^3J_{PC}$ = 24.8 Hz, (Ph$_2$P)H*C*C*C*Me$_2$), 50.8 (d, $^1J_{PC}$ = 44.5 Hz, (Ph$_2$P)*C*CCMe$_2$). Anal. Calcd for $C_{23}H_{17}Fe_2O_6P_2$: C, 51.92; H, 3.22. Found: C, 51.43; H, 2.98.

Preparation of [Fe$_4$(CO)$_{11}$(*μ*-PPh$_2$)$_2$(*μ*-*η*^{2}:*η*^{3}:*η*^{2}:*η*^{1}-C$_α$H$_2$C$_β$C$_γ$HC$_δ$HC$_ε$HC$_φ$H)] (8). Heating a toluene solution of [Fe$_2$(CO)$_6$(*μ*-PPh$_2$){*μ*-*η*^{1}:*η*^{2}-(H)C═C═CH$_2$}] (**1a**; 0.200 g, 0.4 mmol) at reflux for 2 h resulted in a gradual color change from red to deep orange. The solution was cooled to room temperature, and the solvent was removed under reduced pressure to leave a dark oily residue. The residue was extracted into dichloromethane and absorbed onto deactivated alumina, placed on a 300 × 30 mm column, and eluted with *n*-hexane/dichloromethane (70:30, v/v) to give a single major product identified as **8**. Crystallization from methanol/dichloromethane gave orange-red crystals of **8** in 55% yield (0.107 g). IR (*ν*-(CO), cm^{-1}, C_6H_{14}): 2063 m, 2046 s, 2029 s, 2005 s, 2000 m, 1984 s, 1973 w, 1946 w. ^{31}P{^{1}H} NMR (121.5 MHz, $CDCl_3$, *δ*): 174.3 (s, PPh$_2$), 173.7 (s, PPh$_2$). ^{1}H NMR (500.1 MHz, $CDCl_3$, *δ*): 8.53 (dd, J_{PH} = 12.8 Hz, $^3J_{HH}$ = 6.7 Hz, 1H, C$_φ$H), 7.57−7.14 (m, 10H, C$_6$H$_5$), 5.21 (br t, $^3J_{HH} = {}^3J_{PH}$ = 5.8 Hz, 1H, C$_γ$H), 3.59 (ddd, $^3J_{HH}$ = 4.6 Hz, $^3J_{HH}$ = 9.5 Hz, $^3J_{PH}$ = 13.8 Hz, 1H, C$_ε$H), 2.98 (t, $^3J_{HH} = {}^3J_{HH}$ = 9.1 Hz, 1H, C$_δ$H), 2.78 (dd, $^2J_{HH}$ = 4.9 Hz, $^3J_{PH}$ = 11.3 Hz, 1H, C$_α$H), 1.95 (br t, $^2J_{HH} = {}^3J_{PH}$ = 4.9 Hz, 1H, C$_α$H). ^{13}C{^{1}H} NMR (125.65 MHz, $CDCl_3$, *δ*): 214.7 (d, $^2J_{PC}$ = 7.3 Hz, *C*O), 214.7 (d, $^2J_{PC}$ = 14.4 Hz, *C*O), 211.9 (s, *C*O), 177.1 (d, $^2J_{PC}$ = 26.9 Hz, C$_β$), 150.6 (d, $^2J_{PC}$ = 27.9 Hz, C$_φ$), 140.2−128.0 (m, C$_6$H$_5$), 96.3 (d, $^2J_{PC}$ = 24.8 Hz, C$_ε$), 76.4 (s, C$_γ$), 75.2 (s, C$_δ$), 39.8 (d, $^2J_{PC}$ = 9.3 Hz, C$_α$). Anal. Calcd for $C_{41}H_{26}Fe_4O_{11}P_2$: C, 50.25; H, 2.67. Found: C; 50.43; H, 2.61.

Crystal Structure Determination of 4a$_1$, 4b$_2$, and 6−8. Measurements were made on a Bruker AXS SMART CCD diffractometer for **4a$_1$**, **4b$_2$**, and **6** and on a Nicolet R3mV four-circle diffractometer for **7** and **8**, using graphite-monochromated Mo Kα radiation (*λ* = 0.717 03 Å). Intensities were corrected semiempirically (based on symmetry-equivalent and repeated reflections and on azimuthal scan measurements), except for **8**. The structures were solved by direct methods and refined on F^2 values for all unique data by full-matrix least squares. Table 4 gives further details. Non-hydrogen atoms were refined anisotropically. H atoms were constrained, except for those attached to C(1) and C(3) in **4a$_1$** and **4b$_2$** and those attached to C(1) in **6**. Programs used were Bruker AXS SMART and SAINT for diffractometer control and frame integration,[32] Bruker SHELXTL[33] for structure solution, refinement, and molecular graphics, and local programs.

Acknowledgment. We thank the University of Newcastle upon Tyne for financial support, the Nuffield Foundation and the Royal Society for grants (S.D.), and the EPSRC for funding for a diffractometer (W.C.). We thank Dr A. E. Aliev for help with EXSY experiments. S.D. thanks Miss Gina Valks for all her support.

Supporting Information Available: For **4a$_1$, 4b$_2$**, and **6−8** details of the structure determination, non-hydrogen atomic positional parameters, all bond distances and angles, anisotropic displacement parameters, and hydrogen atomic coordinates. This material is available free of charge via the Internet at http://pubs.acs.org. Observed and calculated structure factor tables are available from the authors upon request.

OM000702X

(32) SMART and SAINT software for CCD diffractometers, Bruker AXS Inc., Madison, WI, 1994.
(33) Sheldrick, G. M. *SHELXTL User Manual*, version 5; Bruker AXS Inc.: Madison, WI, 1994.